AD-A049 294 CAMBRIDGE UNIV (ENGLAND) DEPT OF ENGINEERING F/G 11/6
FRACTURE-MECHANISM MAPS FOR PURE IRON AND TWO STAINLESS STEELS.(U)
OCT 77 M F ASHBY DA-ERO-76-G-060
UNCLASSIFIED NL

1 of 1
AD A049 294

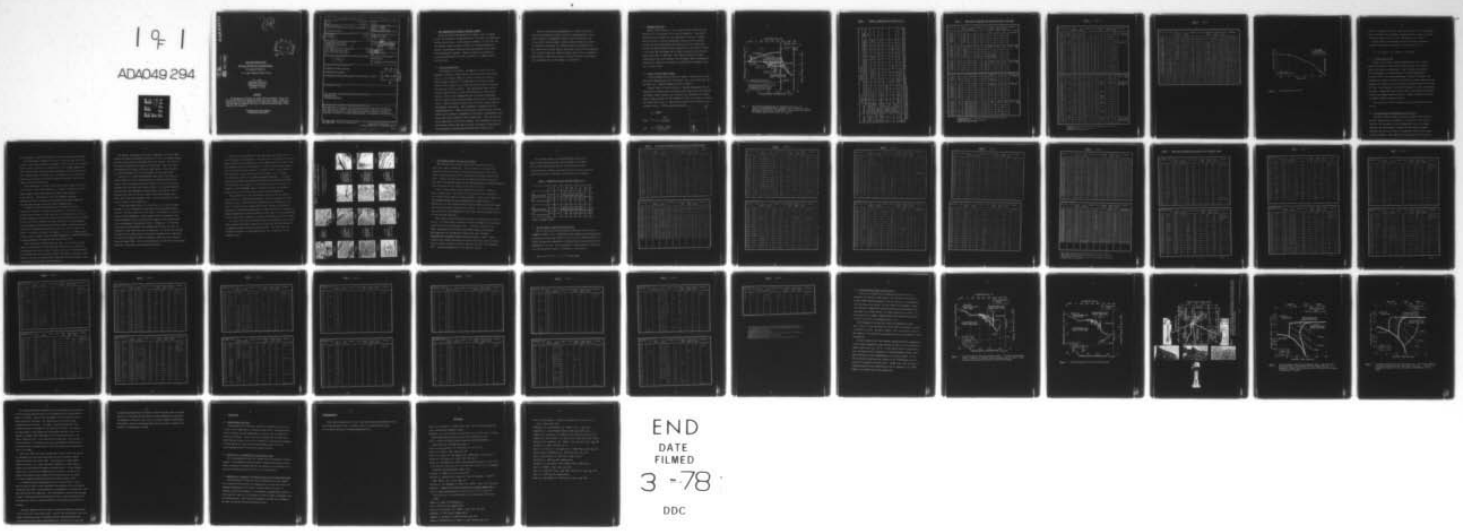

END
DATE FILMED
3-78
DDC

FRACTURE-MECHANISM MAPS

FOR PURE IRON AND TWO STAINLESS STEELS

1ST YEAR-END REPORT ON

U.S. ARMY CONTRACT DAERO-7-G-060

M.F. Ashby
Cambridge University
Engineering Department
Trumpington Street
Cambridge CB2 1PZ

ABSTRACT

The mechanism of fracture of round tensile specimens of pure iron and of type 304 and 316 stainless steel have been studied. These new observations have been combined with a large body of published observation and used to construct two sorts of *fracture mechanism maps*, which summarise the behaviour.

SECURITY CLASSIFICATION OF THIS PAGE (When Data Entered)

REPORT DOCUMENTATION PAGE

READ INSTRUCTIONS BEFORE COMPLETING FORM

1. REPORT NUMBER (67)

2. GOVT ACCESSION NO. (and)

3. RECIPIENT'S CATALOG NUMBER (9)

4. TITLE (and Subtitle)
FRACTURE-MECHANISM MAPS FOR PURE IRON & TWO STAINLESS STEELS

5. TYPE OF REPORT & PERIOD COVERED
ANNUAL REPORT.
OCT 76 → OCT 77

6. PERFORMING ORG. REPORT NUMBER

7. AUTHOR(s) (10)
M.F. ASHBY

8. CONTRACT OR GRANT NUMBER(s) (15)
DAERO-76-G-060 new

9. PERFORMING ORGANIZATION NAME AND ADDRESS
ENGINEERING DEPARTMENT
UNIVERSITY OF CAMBRIDGE
CAMBRIDGE, U.K.

10. PROGRAM ELEMENT, PROJECT, TASK AREA & WORK UNIT NUMBERS (16)
6.11.02A-1T161102BH57-04
DD-595 (17)

11. CONTROLLING OFFICE NAME AND ADDRESS (11)
U.S. ARMY R&S GROUP (EUR)
BOX 65 FPO NEW YORK 09510

12. REPORT DATE
OCTOBER 77

13. NUMBER OF PAGES
45

14. MONITORING AGENCY NAME & ADDRESS (if different from Controlling Office) (12) 46p.

15. SECURITY CLASS. (of this report)
UNCLASSIFIED

15a. DECLASSIFICATION/DOWNGRADING SCHEDULE

16. DISTRIBUTION STATEMENT (of this Report)
APPROVED FOR PUBLIC RELEASE
DISTRIBUTION UNLIMITED

17. DISTRIBUTION STATEMENT (of the abstract entered in Block 20, if different from Report)

18. SUPPLEMENTARY NOTES

19. KEY WORDS (Continue on reverse side if necessary and identify by block number)
FRACTURE MAPS
FRACTURE MECHANISMS

20. ABSTRACT (Continue on reverse side if necessary and identify by block number)
The mechanisms of fracture of round tensile specimens of pure iron and of type 304 and 316 stainless steel have been studied. These new observations have been combined with a large body of published observation and used to construct two sorts of fracture mechanism maps, which summarize the behavior.

DD FORM 1 JAN 73 1473 EDITION OF 1 NOV 65 IS OBSOLETE

UNCLASSIFIED 400 081

SECURITY CLASSIFICATION OF THIS PAGE (When Data Entered)

AB

1. THE CONSTRUCTION OF EMPIRICAL FRACTURE DIAGRAMS

Steels can fracture during monotonic loading in one of a number of ways: by cleavage, by transgranular ductile fracture, by intergranular fracture, and so forth. In this report we assemble, for pure iron, and two stainless steels, the data on failure of round bar specimens in tension, identifying the regime of stress and temperature over which a given mechanism is dominant. Some of the data is new; much of it is from work published in the open literature or in company reports and data sheets.

1.1 Method of Construction

The procedure is as follows. We tabulate, for each test, the *homologous temperature* (T/T_M) and the *normalised tensile stress* (σ_n/E; where σ_n is the nominal stress in a creep or tensile test and E is Young's modulus, adjusted to the temperature of the test), together with the *time-to-fracture* (t_r in secs) and *strain-to-fracture* (ε_f) and the reduction in area at failure. The creep-fracture data refer to tests at constant load; σ_n is the load divided by the initial cross-section. Tests at lower temperatures were at constant displacement rate; for these we have used the ultimate tensile stress to characterise failure. Then we attempt to assign a *mode of failure* to each, based on fractographic observations. This information is assembled into the diagrams shown below. Those for the stainless steels show four *mechanism-fields*: ductile fracture, transgranular creep failure, intergranular creep failure and rupture (necking to zero cross-section). Those for pure iron show an additional field: that of cleavage. The fractography of pure iron has been more detailed than that for steels, and suggests subdivisions of the intergranular creep-fracture field which are described later.

There are difficulties and ambiguities in a study of this sort. There is the influence of purity: strictly, a diagram applies to one purity of metal, or composition of alloy, with one grain size, and in one state of heat-treatment. Specimen shape is important: rupture is favoured in thin sheet, for instance, because the conditions are more nearly those of plane stress, and because of this we have considered only data from round bars, tested in tension, with a ratio of diameter to gauge length of about 1:10. In spite of the difficulties, we have found that the general form of the diagram is reproducible.

2. NOMINALLY PURE IRON

Studies of the fracture of iron in simple tension extend from near absolute zero to nine-tenths of its melting temperature. From them we know that iron can exhibit all the common modes of failure: cleavage, ductile fracture, trans and intergranular creep fracture and rupture. We know also that intergranular creep fracture can occur in more than one way; the grain-boundary cavities responsible for this mode of failure at low stress are lens-shaped; but at higher stresses their perifery becomes finger-like, or wedge-like. The overall behaviour is further complicated by two crystallographic and one magnetic phase transformation. The map which summarises the fracture of round tensile specimens of pure iron is shown as Fig. 1.

2.1 Data on which the Map is Based

We have assembled fracture data for a number of nominally pure irons: Ferrovac-E, BISRA-AH grade iron, Electrolytic iron, zone refined (ZR) iron, and Armco Iron. Chemical analyses are given in Table 1.

The data itself is listed in Table 2. Absolute temperatures (T) were normalised by dividing them by the melting point (T_M) of pure iron (1810 K). The nominal tensile stresses (σ_n) at fracture were normalised by dividing them by Young's modulus E at the temperature of the test, using, for ferrite, the values shown in Fig. 2. These were calculated from the single crystal constants of Dever (1972) using the expressions

$$E = \sqrt{E'E''}$$

where $$E' = C_{11} - \frac{2C_{12}^2}{C_{11} + C_{12}}$$

and $$E'' = \frac{C_{44}(3C_{12} - 2C_{44})}{C_{12} + C_{44}}$$

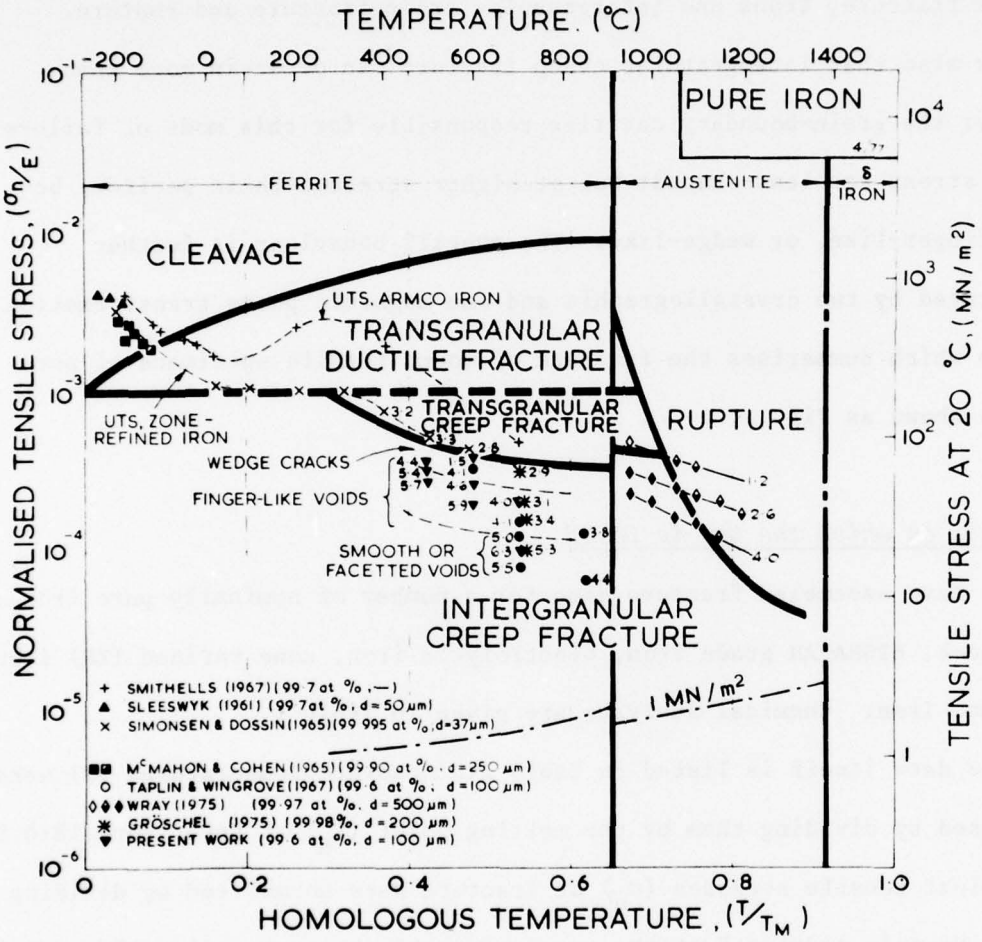

Fig. 1 The fracture-mechanism map for nominally pure iron. It shows five mechanism-fields: cleavage, ductile fracture, transgranular creep fracture, intergranular creep fracture and rupture. The numbers against data points are $\log_{10} t_f$.

TABLE 1 CHEMICAL COMPOSITIONS OF IRONS OF FIG. 1

Material	Reference	Purity		Species (p.p.m.)																	
		At %	Wt %	C	O	N	H	Si	P	S	Mn	Ni	Cr	Mo	V	Co	W	Al	Sn	Cu	Other
Low carbon Ferrovac-E	McMahon and Cohen (1965)	99.88	99.91	327	70	8	-	-	-	-	-	-	-	-	-	-	-	-	-	-	820
Armco iron	Sleeswyk(1961) Smithells(1967)	99.76	99.82	650	-	-	-	-	70	370	240	-	-	-	200	-	-	-	-	880	-
99.98 % pure iron	Gröschel (1976)	-	-	-	-	-	-	-	-	-	-	-	-	-	-	-	-	-	-	-	-
Z.R. electrolytic iron	Simonsen and Dossin (1965)	99.997	99.999	20	2	5	-	1	-	1	-	-	-	-	-	-	-	-	-	2	-
B.I.S.R.A. A.H. iron	Taplin and Wingrove (1967) and present study	99.63	99.90	230	1470	2000	-	-	-	-	20	-	-	-	-	-	-	-	-	-	-
Ferrovac-E	Westwood (1976) and Westwood and Taplin (1974)	99.87	99.92	373	42	6	33	100	36	88	-	238	11	6	44	38	30	207	9	9	-
Z.R. iron	Wray (1975)	99.991	99.996	15	7	8	-	50	.8	.7	1	-	-	-	-	-	-	-	-	-	-
Electrolytic iron	Wray (1975)	99.97	99.98	80	20	18	-	20	30	50	80	-	-	-	-	-	-	--	-	-	-

* This column is not necessarily exclusive of the preceding species. It is assumed that elements in this column have atomic weights near that of iron for purposes of calculating purities.

TABLE 2 DATA USED TO CONSTRUCT THE MAP FOR NOMINALLY PURE IRON

log σ/E	T/T_m	log t_f (sec.)	$\dot{\varepsilon}_{ss}$ (sec^{-1})	ln A_o/A_f	ln l_f/l_o	Fracture Type	Testing Mode	Grain Dia. (μm.)	Reference
-3.993	0.545	5.26	-	-	-	GBC[+]	Creep	208[*]	Gröschel (1975)
-3.943	"	4.26	-	-	-	"	"	"	"
-3.785	"	3.41	-	-	-	"	"	"	"
-3.686	"	3.08	-	-	-	"	"	"	"
-3.487	"	2.89	-	-	-	"	"	"	"
-2.540	0.043	0.829	5.0×10^{-4}	.05	.05	Cleavage	CDR[**]	250	McMahon and Cohen (1965)
-2.662	0.051	0.827	"	.05	.07	"	"	"	"
-2.557	0.057	0.848	"	.13	.13	"	"	"	"
-2.634	0.062	0.949	"	.51	.27	"	"	"	"
-2.694	0.073	0.998	"	1.04	.32	2 % Fibrous	"	"	"
-2.724	0.085	1.034	"	1.56	.37	30 % Fibrous	"	"	"
-2.962	.162	3.2	3.3×10^{-4}	-	.44	Rupture	CDR	37[*]	Simonsen and Dossi (1955)
-2.995	.206	3.2	"	-	.43	"	"	"	
-2.990	.267	3.0	"	-	.29	"	"	"	"
-3.006	.322	3.0	"	-	.30	"	"	"	
-3.121	.371	3.2	"	-	.38	"	"	"	"
-3.293	.427	3.3	3.3×10^{-4}	-	.46	Rupture	CDR	37[*]	Simonsen and Dossi (1965) cont.
-3.369	.477	2.8	"	-	.18	"	"	"	
-2.481	.0425	3.0	"	-	.26	Fibrous	"	"	"
-2.379	.018	-	1×10^{-4}	-	-	Cleavage	CDR	43	Sleeswyk (1961)
-2.391	.026	-	"	-	-	"	"	"	"
-2.404	.033	-	"	-	-	"	"	"	"
-2.409	.034	-	"	-	-	"	"	"	"
-2.420	.036	-	"	-	-	"	"	"	"
-2.405	.041	-	"	-	-	"	"	"	"
-2.439	.049	-	"	-	-	"	"	"	"
-3.820	0.538	4.068	1.64×10^{-5}	-	.27	GBC	CLC[++]	100[*]	Taplin and Wingrove (1967)
-3.863	"	4.255	6.39×10^{-6}	-	.17	"	"	"	"
-3.911	"	4.971	6.94×10^{-7}	-	.13	"	"	"	"
-4.100	"	5.448	3.06×10^{-7}	-	.11	"	"	"	"
-3.514	0.482	4.857	5.56×10^{-6}	-	.34	"	CDR	"	"
-3.487	"	4.051	4.44×10^{-5}	-	.41	"	"	"	"
-3.744	0.538	4.369	5.56×10^{-6}	-	.12	"	"	"	"

+ Grain boundary cavitation was observed, but was not necessarily the cause of fracture.
* Initial grain size.
** Constant displacement-rate, uniaxial tensile test.
++ Constant load, uniaxial creep test.

TABLE 2 (cont.)

log σ/E	T/T_m	log t_f (sec.)	$\dot{\epsilon}_{ss}$ (sec^{-1})	ln A_o/A_f	ln l_f/l_o	Fracture Type	Testing Mode	Grain Dia. (μm)	Reference
-3.695	0.538	3.630	4.44×10^{-5}	-	.17	GBC	CDR	100*	Taplin and Wingrove (1967) /cont.
-4.183	0.620	4.369	5.56×10^{-6}	-	.12	"	"	"	"
-3.882	"	3.800	4.44×10^{-5}	-	.25	"	"	"	"
-3.994	0.538	5.709	8.8×10^{-7}	.60	.37	GBC	CLC	80*	Westwood (1976)
-3.916	"	5.164	5.1×10^{-6}	.80	.56	"	"	"	"
-3.789	"	4.267	3.9×10^{-5}	1.20	.54	"	"	"	
-3.994	"	5.279	3.9×10^{-6}	1.31	.55	"	"	150*	"
-3.916	"	5.218	4.7×10^{-6}	1.20	.58	"	"	"	"
-3.848	"	4.561	2.3×10^{-5}	1.51	.61	"	"	"	"
-3.789	"	4.124	7.4×10^{-5}	2.12	.68	"	"	"	"
-3.994	"	5.174	3.8×10^{-6}	.76	.44	"	"	300*	"
-3.916	"	4.799	1.1×10^{-5}	.87	.53	"	"	"	"
-3.848	"	4.183	4.9×10^{-5}	1.39	.55	"	"	"	"
-3.789	"	4.021	6.7×10^{-5}	1.27	.53	"	"	"	"
-3.994	"	5.675	1.9×10^{-6}	2.12	.63	"	"	500*	"
-3.916	"	5.131	6.7×10^{-6}	2.30	.64	"	"	"	"
-3.848	"	4.575	2.5×10^{-5}	2.30	.66	"	"	"	"
-3.789	"	3.610	2.5×10^{-4}	2.30	.71	"	"	"	"
-3.919	0.538	4.857	7.8×10^{-6}	1.39	.65	GBC	CLC	80*	Westwood and Taplin (1974)
-4.156	"	4.954	3.3×10^{-6}	.51	.26	"	CDR	75*	"
-3.316	.676	1.11	2.3×10^{-2}	3.51	.26	Fibrous	CDR	500*	Wray (1975) and Wray (1975 a) and Wray (1977)
-3.508	"	2.66	6.7×10^{-4}	1.27	.27	GBC	"	"	
-3.649	"	3.92	2.8×10^{-5}	.69	.21	"	"	"	"
-3.439	.703	-	2.3×10^{-2}	-	-	-	"	"	"
-3.550	"	2.67	6.7×10^{-4}	2.53	.27	GBC	"	"	"
-3.700	"	3.95	2.8×10^{-5}	1.61	.22	"	"	"	"
-3.453	.731	1.28	2.3×10^{-2}	∞	.36	Rupture	"	"	"
-3.606	"	2.62	6.7×10^{-4}	4.61	.25	GBC	"	"	"
-3.791	"	4.09	2.8×10^{-5}	2.53	.29	"	"	"	"
-3.477	.759	1.30	2.3×10^{-2}	∞	.37	Rupture	"	"	"
-3.653	"	2.71	6.7×10^{-4}	∞	.29	"	"	"	"
-3.820	"	4.20	2.8×10^{-5}	2.30	.37	GBC	"	"	"
-3.511	.786	1.32	2.3×10^{-2}	-	.39	-	"	"	"
-3.694	"	2.72	6.7×10^{-4}	∞	.30	Rupture	"	"	"
-3.932	"	4.12	2.8×10^{-5}	∞	.31	"	"	"	"
-3.564	.814	-	2.3×10^{-2}	-	-	-	"	"	"
-3.768	.814	2.65	6.7×10^{-4}	∞	.26	Rupture	CDR	500*	Wray (1975) and Wray (1975 a) and Wray (1977)/cont.
-4.041	"	-	2.8×10^{-5}	-	-	-	"	"	

+ Grain boundary cavitation was observed, but was not necessarily the cause of fracture.
* Initial grain size.
** Constant displacement-rate, uniaxial tensile test.
++ Constant load, uniaxial creep test.

TABLE 2 (cont.)

log σ/E	T/T_m	log t_f (sec.)	$\dot{\epsilon}_{ss}$ ($sec.^{-1}$)	ln A_o/A_f	ln l_f/l_o	Fracture Type	Testing Mode	Grain Dia. (μm.)	Reference
-3.443	.427	4.374	4.3×10^{-6}	.59	.18	-	CLC	100	Present Work
-3.461	"	4.948	2.1×10^{-6}	.103	.28	-	"	"	"
-3.499	"	5.412	5.1×10^{-7}	.54	.23	-	"	"	"
-3.554	"	5.737	1.5×10^{-7}	.45	.13	-	"	"	"
-3.580	.483	4.580	4.3×10^{-7}	.53	.21	IG/TG	"	"	"
-3.605	"	4.732	1.9×10^{-7}	.47	.08	IG/TG	"	"	"
-3.626	"	5.070	3.1×10^{-7}	.32	.07	IG/TG	"	"	"
-3.648	"	4.930	5.9×10^{-7}	.46	.08	IG	"	"	"
-3.716	"	5.930	1.4×10^{-7}	.40	.15	-	"	"	"
> -3.30	.539	0.0	-	1.64	-	TG	"	"	"
-3.678	"	3.981	1.0×10^{-5}	1.03	.20	IG/TG	"	"	"
-3.712	"	4.174	7.7×10^{-6}	.98	.20	IG/TG	"	"	"
-3.732	"	4.657	2.3×10^{-6}	.28	.11	IG	"	"	"
-3.857	"	5.603	1.6×10^{-7}	.24	.08	IG	"	"	"
-3.980	"	>6.256	2.2×10^{-8}	> .09	>.04	IG	"	"	"
-	.300	3.08	4.8×10^{-5}	2.16	.42	TG	CDR	"	"
-2.923	.164	3.05	4.8×10^{-5}	1.98	.30	IG	"	"	"
-2.413	.051	-	-	.00	.00	CLEAVAGE	"	-	Smithells (1967)
-2.577	.085	-	-	1.14	.16	-	"	-	"
-2.630	.096	-	-	1.20	.24	-	"	-	"
-2.659	.112	-	-	1.27	.32	-	"	-	"
-2.673	.123	-	-	1.35	.36	-	"	-	"
-2.722	.140	-	-	1.39	.35	-	"	-	"
-2.803	.162	-	-	1.31	.25	-	"	-	"
-2.761	.162	-	-	1.17	.37	-	"	-	"
-2.612	.261	-	-	.78	.24	-	"	-	"
-2.735	.372	-	-	1.11	.14	-	"	-	"
-3.135	.482	-	-	.67	.29	-	"	-	"
-3.334	.538	-	-	.80	.43	-	"	-	"

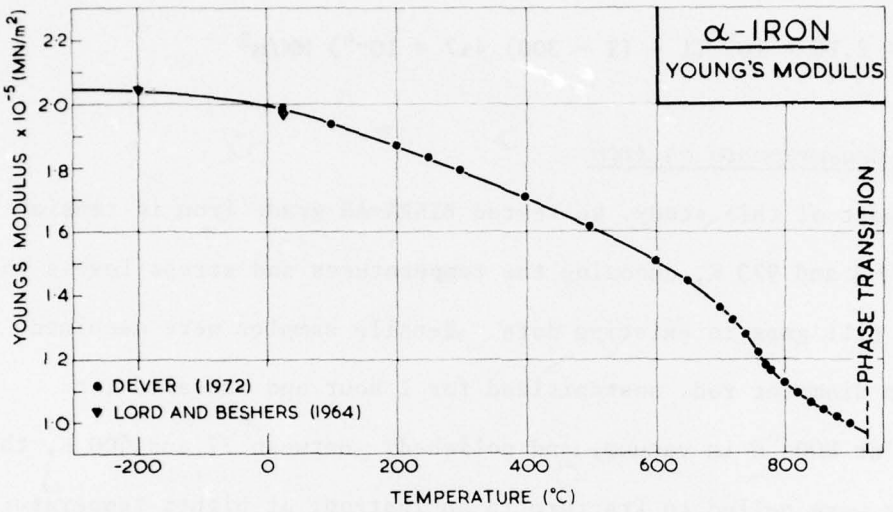

Fig. 2 Young's modulus for α-iron.

(This is a statement of E for an untextured polycrystal. At room temperature, it predicts 1.98×10^5 MN/m^2, compared with the average of several polycrystal studies of $1.97 (\pm .04) \times 10^5$ MN/m^2 (A.S.M., 1961)).

Young's modulus for austenite was derived from the measurements of Köster (1948), and is described, to first order in T, by:

$$E = 2.16 \times 10^5 \, (1 - (T - 300) \, 4.7 \times 10^{-4}) \text{ MN/m}^2$$

2.2 *New Measurements on Iron*

As part of this study, we tested BISRA-AH grade iron in tension between 77 K and 973 K, choosing the temperatures and stress levels to check or fill gaps in existing data. Tensile samples were machined from 6 mm diameter rod, austenitized for 1 hour and annealed for 24 hours at 800 ^{o}C in vacuum, and polished. Between 77 and 400 K, the specimens were pulled to fracture in an Instron; at higher temperatures the specimens were tested in creep at constant load under vacuum of better than 10^{-5} torr. The mechanism of fracture was examined by optical and scanning microscopy. Samples were then cooled to -196 ^{o}C and fractured again about 3 mm from the original fracture surface to examine the shapes of cavities on boundaries behind the fracture surface.

The results are included in Table 2, and are described in the next section.

2.3 *The Fracture Map for Nominally Pure Iron (Fig. 1)*

The data of Table 2 appear on the map as symbols (identifying the source), labelled with the logarithm, to the base 10, of the time-to-fracture. Filled symbols in the low temperature end of the diagram mean that the observed mode of fracture was by cleavage; elsewhere they mean that one of a variety of intergranular creep-fracture mechanisms was dominant. Open symbols and crosses means that the fracture

was transgranular. Half-filled symbols indicate that rupture was observed.

The fractographic information was used to divide the maps into *fields* in which a given mode of fracture is dominant. Below about 0.1 T_M (- 100 ^oC) failure of iron of Ferrovac E or Armco purity is by cleavage (McMahon and Cohen, 1965; Sleeswyk, 1961) apparently nucleated by the slip-induced cracking of carbides which are present even in this grade of iron. When these carbides are removed by zone refining (Simonsen and Dossin, 1965) the iron remains ductile to below 0.06 T_M.

As the temperature is raised, the fracture surface changes from 100 % cleavage (solid squares and triangles) to a mixture of cleavage facets and fibrous dimples, (half-filled square) and then to 100 % fibrous or ductile fracture. The position of the field boundary separating cleavage from ductile fracture has been inferred from these changes and from the large increase in ductility which accompanies them.

Between 0.1 and 0.3 T_M the material fails rapidly by a ductile cup-and-cone fracture, at a nominal stress equal to the U.T.S.; at even slightly lower stresses, it fails only after a very long time or not at all. The lower boundary of the ductile fracture field (broken heavy line) is based on the U.T.S. data of Simonsen and Dossin (1965) and is in good agreement with the boundary, inferred by Frost and Ashby (1975), separating power-law creep from low-temperature plasticity in pure iron. Data for Armco iron, which is less pure, are shown on the diagram. Its U.T.S. (+ symbols) shows a hump at 200 ^oC, probably caused by carbon segregation or carbide precipitation. The field boundaries are based on data from the purer iron.

Above 0.3 T_M, iron exhibits power-law creep. If the stress is high enough to cause fracture in less than about 10^3 seconds, the fracture is transgranular; but as the stress is reduced, there is a well-defined change to an intergranular mode of fracture (Taplin and Wingrove, 1967; Wray, 1965; Gröschel, 1975; and our present work), from which the lower boundary of the transgranular creep fracture field was deduced.

The magnetic phase change at the Curie temperature, 0.57 T_M, changes slightly the moduli and diffusion coefficients of iron, and thereby changes the creep rates (see Frost and Ashby, 1975, for a review). The effect on the fracture behaviour is too small to be observable. The α to γ phase transformation at 0.65 T_M, on the other hand, causes a large increase in t_f, and a discontinuity in the field boundary, as the figure shows.

Above the α to γ phase transformation, Wray (1975) found that zone refined (99.997 at %) iron recrystallised as it deformed and failed by rupture. When he examined electrolytic (99.97 at %) iron, with a purity comparable with the other irons listed in Table 2, he found transgranular creep fracture (open diamonds) and intergranular creep fracture (solid diamonds) below about 0.7 T_M, and rupture (half-solid diamonds) above (Wray, 1975, 1976; Wray and Holmes, 1975). The field boundaries in this region are based on his observations.

Iron has the property that, if, after creep, it is cooled in liquid nitrogen, it can be fractured in a way which reveals the grain-boundary cavities. This has allowed the cavity shape to be studied as a function of stress, time and temperature. These studies (Taplin and Wingrove, 1967; Cane and Greenwood, 1975; our present work) suggest certain sub-divisions of the intergranular creep-fracture field. In summary, it is found that, just below the field boundary with transgranular fracture, the voids are irregular in shape, and often crack or wedge-like. At rather lower stresses, they grow in the boundary plane as thin discs, sometimes with a finger-like perifery first reported by Taplin and Wingrove (1967) and later studied by Fields and Ashby (1976). At still lower stresses, the cavities are more nearly spherical or lens-like, and are frequently facetted.

Some of our own observations of the cavity shapes are shown in Fig. 3, which illustrates this progression. The first pair of micrographs (top, left) shows inclusions on grain boundaries of the BISRA-AH grade iron, before creep. The subsequent pairs show the appearance of typical grain boundary surfaces, some 3 mm from the actual creep-fracture surface, and in a plane normal to the tensile axis, as the creep stress was increased. At low stresses (< 14 MN/m^2) the cavities are roughly equiaxed and facetted. At higher stresses (18-26 MN/m^2) they become flatter and more disc-shaped with finger-like protrusions at the edges. At still higher stresses, the density of boundary cavities decreases, there is increasing evidence for extensive plastic flow, and the creep fracture itself becomes transgranular.

These subdivisions of the intergranular fracture field are shown on the map (Fig. 1). Although such changes are less well documented in other materials, there is every reason for thinking that the transition, as the stress is raised, from an equiaxed cavity shape, through a disk-like one (perhaps with finger-like protrusions) to a wedge-like crack is a general one. Since the growth of the cavities depends on their shape, the law governing the fracture time, and its dependence on stress and temperature, will also change.

It will be clear from this discussion that field boundaries have a finite width in which mixed modes of fracture are found; and that the positions of the boundaries depend on purity or alloy content. This effect has been documented elsewhere for nickel-based alloys, and is found, too, in the stainless steels.

Fig. 3 CAVITY MORPHOLOGY IN IRON AT 975 KELVIN AS A FUNCTION OF ENGINEERING STRESS (σ_o).

SPECIMEN BROKEN OPEN 3MM FROM ACTUAL FRACTURE SURFACE IN A PLANE PERPENDICULAR TO THE TENSILE AXIS

50 μm

$\sigma_o = 0$

SMOOTH GRAIN BOUNDARIES WITH INCLUSIONS. NO CAVITATION.

12.5 μm

50 μm

$\sigma_o = 14.1$ MPa

COPIOUS CAVITATION ON GRAIN BOUNDARIES. *NUCLEATION AT* INCLUSIONS. ANGULAR, ANISOTROPIC CAVITIES.

TIME TO FAIL > 500 HRS.

70 μm

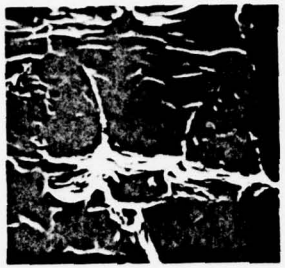

5 μm

$\sigma_o = 26.1$ MPa

MANY GRAIN BOUNDARY CAVITIES WITH FINGER-LIKE FRONTS. SOME SLIP BANDS AND DUCTILE FRACTURE DIMPLES VISIBLE.

TIME TO FAIL = 4.15 HRS.

10 μm

20 μm

$\sigma_o = 18.7$ MPa

SMALL, ROUND VOIDS COALESCE TO FORM A *FEW* LARGE CRACKS WITH FINGER-LIKE FRONTS.

TIME TO FAIL = 111.5 HRS.

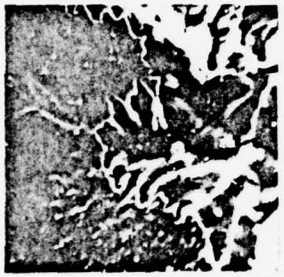

20 μm

10 μm

$\sigma = 28.3$ MPa.

ABUNDANT DUCTILE FRACTURE DIMPLES AND SLIP BANDS. PECULIAR, ALIGNED CAVITIES APPEAR OCCASIONALLY ON GRAIN BOUNDARIES.

TIME TO FAIL = 2.66 HRS.

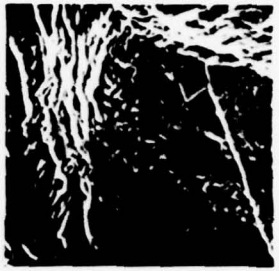

20 μm

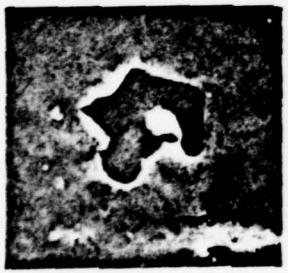

5 μm

$\sigma_o = 25.0$ MPa.

CAVITIES AT ALL STAGES SHOW FINGER-LIKE FRONTS.

TIME TO FAIL = 12.6 HRS.

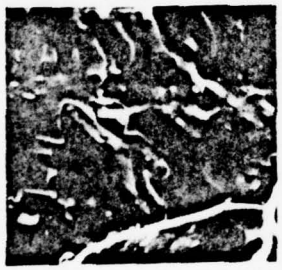

12.5 μm

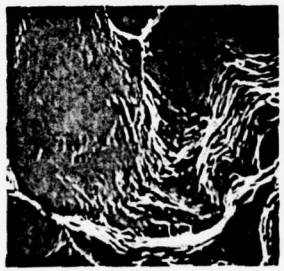

50 μm

$\sigma_o > 50$ MPa.

NO CAVITATION HERE. GRAIN BOUNDARIES RUMPLED BY MANY INTERSECTING SLIP BANDS.

TIME TO FAIL = 10 SEC.

5 μm

3. THE STAINLESS STEELS: 304 and 316 Stainless

The 18-8 austenitic stainless steels find commercial application over a wide range of temperature. They are ductile at cryogenic temperatures, and so can be used in superconducting machinery. They resist aqueous corrosion, and are used for containing and handling chemicals and foods. Finally, they have useful creep strength and oxidation resistance up to 650 ^{o}C, making them attractive for high-temperature load bearing components. Type 304 and type 316 are typical of this series of alloys.

There is some variation in the mechanical properties of different heats of these steels. One reason is the variation in their composition: their specifications permits a certain latitude in alloy content (Table 3). The strength depends, too, on the mechanical and thermal history: an important part of the strength derives from work hardening; and both strength and corrosion resistance depend on heat treatment. For these reasons, data from steels which were homogenised at about 1300 K and then quenched into oil or water have been used here.

There remain certain unexplained variations in creep-ductility of these alloys. It is known that precipitation continues throughout even the longest creep tests of 316, and probably of 304. Typically, carbides of the $M_{23}C_6$ type appear first, and while they slowly coarsen, a grain-boundary sigma-phase (an intermetallic of FeCr type) and a chi-phase (approximating $Fe_{36}C_{12}Mo_{10}$) appear (Weiss and Stickler, 1972). Strain influences the topology and kinetics of the precipitation, and the concentrations of carbon and boron in the alloy may do so also (Lai, 1977; Marshall, 1977). The data assembled here is for low-boron steels.

For all these reasons, the field boundaries shown on the maps for these stainless steels, must be thought of as diffuse. We do not yet know how wide they are or by how much the time-contours may vary, though as the figures show all the data we have reviewed in this study is tolerably well described by the diagrams.

TABLE 3 COMPOSITIONS OF THE STAINLESS STEELS, wt %

	Cr	Ni	C	Si	Mn	P	S	Mo	Fe
304 Permitted Range*	18-20	8-12	.08 max	1.0 max	2.0 max	.045 max	.03 max	-	bal
304 this investigation	18.26	9.51	.05	.29	1.42	.031	.012		bal
316 Permitted Range*	16-18	10-14	.08 max	1.0 max	2.0 max	.045 max	.03 max	2-3	bal
316 this investigation	16.82	11.15	.06	.25	1.68	.035	.015	2.43	bal

* Parr and Hanson (1965)

3.1 *Data for Type 304 and 316 Stainless Steels*

Data for 304 and 316 tensile specimens, machined from bar stock, is assembled in Tables 4 and 5. Temperatures were normalised by dividing by the melting point of pure iron (1810 K) to allow a direct comparison with Fig. 1. Tensile stresses were normalised by dividing them by Young's modulus at the temperature of the test. For this purpose, we used Blackburn's (1972) data for E for 304 and 316, which, if linearised, is described by

$$E(T) = 2.16 \times 10^5 \ (1 - 4.7 \times 10^{-4} \ (T-300)) \ MN/m^2$$

TABLE 4 DATA USED TO CONSTRUCT THE MAPS FOR 304 STAINLESS STEEL

304 Stainless Steel (1)

log σ/E	T/T_m	log t_f (sec.)	$\dot{\epsilon}_{ss}$ (sec^{-1})	ln A_o/A_f	ln l_f/l_o	Fracture Type	Testing Mode	Grain Dia. (μm)	Reference
-2.16	.074	4.06	$3.3x10^{-5}$ *	1.11	.32	-	CDR*	-	Sanderson et al. (1969)
-2.22	.073	4.10	"	1.14	.35	-	"	-	"
-2.24	.096	4.12	"	1.17	.36	-	"	-	"
-2.27	.123	4.19	"	1.24	.41	-	"	-	"
-2.34	.140	4.22	"	1.11	.44	-	"	-	"
-2.38	.151	4.29	"	1.39	.50	-	"	-	"
-2.54	.162	4.34	"	1.49	.54	-	"	-	"
-2.63	.206	4.25	"	1.54	.46	-	"	-	"
-2.65	.261	4.17	"	1.39	.40	-	"	-	"
-2.63	.317	4.13	"	1.19	.37	-	"	-	"
-2.60	.372	4.15	"	1.27	.38	-	"	-	"
-2.61	.427	4.10	"	1.19	.35	-	"	-	"
-2.64	.482	4.10	"	.94	.35	-	"	-	"
-2.79	.538	4.16	"	.94	.39	-	"	-	"
-3.02	.593	4.28	"	.94	.49	-	"	-	"
-2.550	.164	-	-	1.51	.49	-	"	62	Smith et al (1950)
-2.650	.479	-	-	1.02	.30	-	"	"	"
-2.770	.540	-	-	.69	.31	-	"	"	"

304 Stainless Steel (2)

log σ/E	T/T_m	log t_f (sec.)	$\dot{\epsilon}_{ss}$ (sec^{-1})	ln A_o/A_f	ln l_f/l_o	Fracture Type	Testing Mode	Grain Dia. (μm)	Reference
-2.93	.602	-	-	.54	.32	-	CDR	62	Smith et al.(1950)
-2.66	.479	3.76	$1.7x10^{-5}$	.68	.28	TG^{++}	CLC^{+}	"	"
-2.73	"	4.36	$4.9x10^{-6}$	.37	.26	IG^{++}	"	"	"
-2.84	"	5.29	$4.5x10^{-7}$	.33	.15	"	"	"	"
-2.93	"	6.19	$9.9x10^{-8}$	.26	.14	"	"	"	"
-3.00	"	6.76	$2.1x10^{-8}$	.23	.12	"	"	"	"
-2.87	.540	3.22	-	.53	.33	TG^{++}	"	"	"
-2.91	"	3.76	$3.7x10^{-5}$	.43	.32	"	"	"	"
-3.03	"	4.52	$5.3x10^{-6}$	.30	.25	"	"	"	"
-3.15	"	5.24	$4.2x10^{-7}$	.24	.23	IG^{++}	"	"	"
-3.29	"	6.09	$1.6x10^{-7}$	.31	.25	"	"	"	"
-3.35	"	6.72	$3.7x10^{-8}$	.30	.28	"	"	"	"
-3.12	.602	3.39	-	.55	.45	TG^{++}	"	"	"
-3.18	"	3.89	-	.42	.35	"	"	"	"
-3.29	"	4.76	$5.4x10^{-6}$	.39	.35	"	"	"	"
-3.43	"	5.47	$5.7x10^{-7}$	.30	.30	IG^{++}	"	"	"
-3.56	"	6.12	$2.5x10^{-7}$	.32	.28	"	"	"	"
-3.66	"	6.66	$3.5x10^{-8}$	.20	.25	"	"	"	"

TABLE 4 (cont.)

316 Stainless Steel (3)

log σ/E	T/T_m	log t_f (sec.)	$\dot{\epsilon}_{ss}$ (sec^{-1})	ln A_o/A_f	ln l_f/l_o	Fracture Type	Testing Mode	Grain Dia. (μm.)	Reference
-2.570	.417	2.360	-	-	-	TG++	CLC	62	Dulis et al (1953)
-2.640	"	6.080	2.4×10^{-8}	.67	.31	IG++	"	"	"
-2.670	"	6.370	1.6×10^{-8}	.43	.28	"	"	"	"
-2.700	"	6.630	5.6×10^{-9}	.36	.23	"	"	"	"
-2.650	.463	3.360	3.3×10^{-5}	1.47	.39	TG++	"	"	"
-2.680	"	4.360	5.2×10^{-6}	.70	.34	"	"	"	"
-2.750	"	5.120	1.1×10^{-6}	.44	.29	IG++	"	"	"
-2.880	"	6.230	6.4×10^{-8}	.32	.19	"	"	"	"
-2.970	"	6.820	1.5×10^{-8}	.30	.18	"	"	"	"
-2.740	.509	3.060	-	1.00	.45	TG++	"	"	"
-2.850	"	4.320	9.9×10^{-6}	.51	.34	"	"	"	"
-2.940	"	4.970	2.2×10^{-6}	.41	.29	IG++	"	"	"
-3.020	"	5.650	3.7×10^{-7}	.38	.25	"	"	"	"
-3.150	"	6.390	5.6×10^{-8}	.25	.21	"	"	"	"
-3.320	"	7.070	1.3×10^{-8}	.26	.17	"	"	"	"
-2.157	.013	-	-	.56	.39	-	CDR	-	INCO (1974)
-2.217	.040	-	-	.60	.37	-	"	-	"
-2.279	.068	-	-	.66	.39	-	"	-	"

304 Stainless Steel (4)

log σ/E	T/T_m	log t_f (sec.)	$\dot{\epsilon}_{ss}$ (sec^{-1})	ln A_o/A_f	ln l_f/l_o	Fracture Type	Testing Mode	Grain Dia. (μm.)	Reference
-2.339	.096	-	-	.78	.41	-	CDR	-	INCO (1974)
-2.409	.123	-	-	.92	.43	-	"	-	"
-2.501	.151	-	-	1.08	.46	-	"	-	"
-2.556	.165	-	-	1.20	.47	-	"	-	"
-2.970	.455	7.560	-	-	-	-	CREEP+	-	ISO (1969)
-2.990	.460	"	-	-	-	-	"	-	"
-3.020	.466	"	-	-	-	-	"	-	"
-3.050	.471	"	-	-	-	-	"	-	"
-3.080	.477	"	-	-	-	-	"	-	"
-3.110	.482	"	-	-	-	-	"	-	"
-3.140	.488	"	-	-	-	-	"	-	"
-3.170	.493	"	-	-	-	-	"	-	"
-3.210	.499	"	-	-	-	-	"	-	"
-3.320	"	8.030	-	-	-	-	"	-	"
-3.250	.504	7.560	-	-	-	-	"	-	"
-3.360	"	8.030	-	-	-	-	"	-	"
-3.290	.510	7.560	-	-	-	-	"	-	"
-3.400	"	8.030	-	-	-	-	"	-	"

TABLE 4 (cont.)

304 Stainless Steel (5)

log σ/E	T/T_m	log t_f (sec.)	$\dot{\epsilon}_{ss}$ ($sec.^{-1}$)	ln A_o/A_f	ln l_f/l_o	Fracture Type	Testing Mode	Grain Dia. (μm)	Reference
-3.320	.515	7.560	-	-	-	-	CREEP	-	150 (1968)
-3.440	"	8.030	-	-	-	-	"	-	"
-3.350	.521	7.560	-	-	-	-	"	-	"
-3.480	"	8.030	-	-	-	-	"	-	"
-3.390	.527	7.560	-	-	-	-	"	-	"
-3.430	.532	"	-	-	-	-	"	-	"
-3.490	.538	"	-	-	-	-	"	-	"
-2.161	.012	-	-	.96	.37	-	CDR	-	Simmons and Van Echo (1965)
-2.226	.043	-	-	.60	.36	-	"	-	"
-2.220	.049	-	-	.86	.37	-	"	-	"
-2.589	.164	-	-	1.51	.53	-	"	-	"
-2.637	.202	-	-	1.41	.44	-	"	-	"
-2.656	.264	-	-	1.22	.36	-	"	-	"
-2.646	.294	-	-	1.26	.39	-	"	-	"
-2.639	.325	-	-	1.19	.37	-	"	-	"
-2.619	.356	-	-	1.18	.39	-	"	-	"
-2.634	.371	-	-	-	.38	-	"	74	"
-2.614	.387	-	-	1.19	.37	-	"	-	"

304 Stainless Steel (6)

log σ/E	T/T_m	log t_f (sec.)	$\dot{\epsilon}_{ss}$ ($sec.^{-1}$)	ln A_o/A_f	ln l_f/l_o	Fracture Type	Testing Mode	Grain Dia. (μm)	Reference
-2.627	.417	-	-	-	.36	-	CDR	-	Simmons and Van Echo (1965)
-2.624	.448	-	-	1.12	.35	-	"	-	"
-2.647	.479	-	-	.87	.33	-	"	-	"
-2.692	.509	-	-	.65	.29	-	"	-	"
-2.783	.540	-	-	-	.30	-	"	74	"
-2.867	.571	-	-	-	.29	-	"	"	"
-2.976	.601	-	-	.75	.29	-	"	"	"
-3.031	.632	-	-	-	.27	-	"	61	"
-3.255	.693	-	-	-	.39	-	"	"	"
-2.613	.417	5.90	-	-	.34	-	CREEP	-	"
-2.628	"	6.27	-	-	.31	-	"	-	"
-2.651	"	6.50	-	-	.23	-	"	-	"
-2.659	"	6.56	-	-	-	-	"	-	"
-2.675	"	6.96	-	-	.24	-	"	-	"
-2.774	.448	6.195	-	-	-	-	"	-	"
-2.756	.463	5.80	-	-	.13	-	"	74	"
-2.767	"	5.40	-	-	-	-	"	-	"
-2.807	"	6.26	-	-	.14	-	"	74	"

TABLE 4 (cont.)

304 Stainless Steel (2)

log σ/E	T/T_m	log t_f (sec.)	$\dot{\epsilon}_{ss}$ ($sec.^{-1}$)	ln A_o/A_f	ln l_f/l_o	Fracture Type	Testing Mode	Grain Dia. (μm.)	Reference
-2.892	.563	6.93	-	-	.09	-	CREEP	74	Simmons and Van Echo (1963) cont.
-2.937	"	7.22	-	-	.06	-	"	"	"
-2.989	"	7.63	-	-	.06	-	"	"	"
-2.708	.479	3.718	-	-	.29	-	"	62	"
-2.748	"	4.732	-	-	-	-	"	-	"
-2.759	"	4.602	-	-	.29	-	"	62	"
-2.781	"	4.954	-	-	-	-	"	-	"
-2.805	"	5.334	-	-	-	-	"	-	"
-2.817	"	5.567	-	-	.15	-	"	-	"
-2.843	"	5.281	-	-	.15	-	"	62	"
-2.856	"	5.879	-	-	-	-	"	-	"
-2.884	"	6.096	-	-	.25	-	"	-	"
-2.899	"	5.729	-	-	.12	-	"	62	"
-2.922	"	6.556	-	-	-	-	"	-	"
-2.930	"	6.636	-	-	.37	-	"	-	"
-2.955	"	6.055	-	-	.12	-	"	62	"
-2.965	"	6.109	-	-	.15	-	"	"	"
-2.976	"	6.876	-	-	-	-	"	-	"

304 Stainless Steel (3)

log σ/E	T/T_m	log t_f (sec.)	$\dot{\epsilon}_{ss}$ ($sec.^{-1}$)	ln A_o/A_f	ln l_f/l_o	Fracture Type	Testing Mode	Grain Dia. (μm.)	Reference
-3.019	.479	7.212	-	-	-	-	CREEP	-	Simmons and Van Echo (1963) cont.
-3.029	"	6.759	-	-	.11	-	"	62	"
-3.039	"	6.716	-	-	.13	-	"	62	"
-2.751	.494	4.003	-	-	-	-	"	-	"
-3.052	"	6.879	-	-	-	-	"	-	"
-2.743	.509	3.56	-	-	.30	-	"	74	"
-2.777	"	3.56	-	-	-	-	"	-	"
-2.854	"	4.48	-	-	.22	-	"	74	"
-2.868	"	4.76	-	-	-	-	"	-	"
-2.898	"	4.61	-	-	.18	-	"	74	"
-2.906	"	5.87	-	-	.18	-	"	-	"
-2.914	"	5.88	-	-	.15	-	"	74	"
-2.930	"	5.16	-	-	-	-	"	-	"
-2.948	"	5.38	-	-	-	-	"	-	"
-2.984	"	5.70	-	-	-	-	"	-	"
-3.003	"	6.22	-	-	.24	-	"	74	"
-3.023	"	6.33	-	-	.25	-	"	-	"
-3.044	"	6.38	-	-	.22	-	"	-	"

TABLE 4 (cont.)

304 Stainless Steel (9)

log σ/E	T/T_m	log t_f (sec.)	$\dot{\epsilon}_{ss}$ (sec^{-1})	ln A_o/A_f	ln l_f/l_o	Fracture Type	Testing Mode	Grain Dia. (μm.)	Reference
-3.067	.509	6.26	-	-	-	-	CREEP	-	Simmons and Van Echo (1965) cont'd
-3.090	"	6.93	-	-	.28	-	"	74	"
-3.115	"	6.51	-	-	.17	-	"	74	"
-3.128	"	7.58	-	-	.22	-	"	74	"
-3.141	"	6.35	-	-	.11	-	"	62	"
-3.169	"	7.58	-	-	.24	-	"	74	"
-3.199	"	7.32	-	-	.14	-	"	74	"
-3.266	"	7.04	-	-	.15	-	"	74	"
-3.036	.525	5.58	-	-	-	-	"	-	"
-2.852	.540	3.11	-	-	.30	-	"	65	"
-2.931	"	3.73	-	-	.31	-	"	62	"
-2.987	"	4.37	-	-	.37	-	"	72	"
-3.028	"	4.79	-	-	.26	-	"	62	"
-3.074	"	5.15	-	-	.38	-	"	72	"
-3.153	"	5.63	-	-	.39	-	"	62	"
-3.215	"	5.55	-	-	.23	-	"	62	"
-3.232	"	6.41	-	-	.62	-	"	-	"
-3.250	"	5.82	-	-	.18	-	"	72	"
-3.268	"	6.56	-	-	-	-	"	-	"
-3.288	"	6.43	-	-	.33	-	"	62	"
-3.329	"	6.59	-	-	.17	-	"	65	"
-3.375	"	6.73	-	-	.21	-	"	62	"
-3.020	.555	4.33	-	-	-	-	"	-	"
-3.145	"	5.64	-	-	.31	-	"	-	"
-3.207	"	5.69	-	-	.49	-	"	-	"
-3.242	"	6.31	-	-	.39	-	"	72	"
-3.321	"	6.96	-	-	.25	-	"	-	"
-3.356	"	7.37	-	-	.35	-	"	72	"
-3.366	"	7.21	-	-	.36	-	"	72	"
-3.418	"	7.65	-	-	.29	-	"	72	"
-3.446	"	7.56	-	-	.24	-	"	-	"
-2.970	.571	3.23	-	-	.28	-	"	72	"
-3.011	"	4.16	-	-	-	-	"	-	"
-3.082	"	3.92	-	-	.23	-	"	72	"
-3.166	"	4.36	-	-	.23	-	"	72	"
-3.467	"	6.43	-	-	.17	-	"	72	"

304 Stainless Steel (10)

log σ/E	T/T_m	log t_f (sec.)	$\dot{\epsilon}_{ss}$ (sec^{-1})	ln A_o/A_f	ln l_f/l_o	Fracture Type	Testing Mode	Grain Dia. (μm.)	Reference
-3.534	.571	6.60	-	-	.14	-	CREEP	72	Simmons and Van Echo (1965) cont'd
-3.613	"	7.09	-	-	.13	-	"	72	"
-3.303	.586	5.57	-	-	-	-	"	-	"
-3.604	"	7.18	-	-	-	-	"	-	"
-3.118	.601	3.29	-	-	.34	-	"	67	"
-3.181	"	3.83	-	-	.34	-	"	62	"
-3.215	"	4.56	-	-	.68	-	"	-	"
-3.253	"	4.20	-	-	.22	-	"	72	"
-3.295	"	4.88	-	-	.49	-	"	62	"
-3.317	"	4.32	-	-	.17	-	"	72	"
-3.381	"	4.98	-	-	.21	-	"	72	"
-3.391	"	5.59	-	-	.54	-	"	-	"
-3.449	"	5.86	-	-	.43	-	"	62	"
-3.516	"	5.61	-	-	.23	-	"	67	"
-3.546	"	6.36	-	-	-	-	"	-	"
-3.570	"	6.08	-	-	.26	-	"	62	"
-3.596	"	6.78	-	-	.28	-	"	72	"
-3.671	"	6.62	-	-	.25	-	"	62	"
-3.692	"	6.63	-	-	.17	-	"	67	"
-3.285	.617	4.44	-	-	-	-	"	-	"
-3.440	"	5.42	-	-	-	-	"	-	"
-3.577	.632	5.91	-	-	-	-	"	-	"
-3.422	.647	4.72	-	-	-	-	"	-	"
-3.558	.663	5.01	-	-	-	-	"	-	"
-3.655	"	5.58	-	-	-	-	"	-	"
-3.548	.678	4.49	-	-	-	-	"	-	"
-3.538	.693	4.06	-	-	-	-	"	-	"
-3.635	"	4.41	-	-	-	-	"	-	"
-3.360	.814	0.0	5.1×10^{-1}	∞	.43	PUPTURE	CDR	-	Nadai et al (1941)
-3.492	.703	2.80	8.5×10^{-4}	-	.43	-	"	-	"

+ CDR - constant displacement-rate tensile test; CLC - constant load, uniaxial creep test; CREEP - unspecified loading mode, uniaxial creep test.

* This strain-rate was assumed for these tensile tests in order to calculate a time-to-failure from the longitudinal fracture strain.

++ TG (orIG) transgranular (or intergranular) fracture inferred from position in stress and time relative to kink in creep rupture curve.

TABLE 5 DATA USED TO CONSTRUCT THE MAPS FOR 316 STAINLESS STEEL

316 Stainless Steel (1) log σ/E	T/T_m	log t_f (sec.)	$\dot{\epsilon}_{ss}$ ($sec.^{-1}$)	ln A_o/A_f	ln l_f/l_o	Fracture Type	Testing Mode	Grain Dia. (μm.)	Reference
-2.24	.043	4.23	3.3×10^{-5}	1.12	.44	-	CDR*	100	Sanderson
-2.31	.073	4.25	"	1.20	.47	-	"	"	et al. (1969)
-2.36	.096	4.30	"	1.39	.51	-	"	"	
-2.43	.123	4.40	"	1.35	.61	-	"	"	
-2.49	.140	4.42	"	1.35	.63	-	"	"	
-2.51	.151	4.38	"	.97	.59	-	"	"	
-2.57	.162	4.26	"	1.49	.47	-	"	"	
-2.62	.206	4.21	"	1.44	.43	-	"	"	
-2.64	.261	4.16	"	1.39	.39	-	"	"	
-2.61	.317	4.14	"	1.15	.38	-	"	"	
-2.58	.372	4.14	"	1.19	.38	-	"	"	
-2.56	.427	4.13	"	1.07	.37	-	"	"	
-2.60	.482	4.08	"	1.15	.34	-	"	"	
-2.72	.538	4.15	"	.76	.39	-	"	"	
-2.92	.593	4.21	"	1.07	.43	-	"	"	
-2.465	0.165	3.030	5.5×10^{-4}	1.43	.45	-	"	45	Simmons and
-2.553	"	3.073	"	1.34	.49	-	"	-	Van Echo (1965)
-2.568	"	3.008	"	1.28	.49	-	"	-	
-2.580	"	3.086	"	1.57	.51	-	"	65	

316 Stainless Steel (2) log σ/E	T/T_m	log t_f (sec.)	$\dot{\epsilon}_{ss}$ ($sec.^{-1}$)	ln A_o/A_f	ln l_f/l_o	Fracture Type	Testing Mode	Grain Dia. (μm.)	Reference
-2.584	0.165	3.016	5.5×10^{-4}*	-	.46	-	CDR	75	Simmons and
-2.591	"	3.052	"	-	.50	-	"	55	Van Echo (1965)
-2.594	"	3.063	"	-	.48	-	"	130	Cont'd.
-2.602	"	3.060	"	-	.44	-	"	-	
-2.605	0.295	2.903	"	1.17	.36	-	"	45	
-2.574	0.356	2.828	"	1.08	.31	-	"	"	
-2.562	0.387	2.913	"	1.05	.37	-	"	"	
-2.495	0.448	2.922	"	1.11	.38	-	"	"	
-2.539	"	2.851	"	-	.38	-	"	75	
-2.558	"	2.922	"	-	.33	-	"	-	
-2.534	0.463	2.898	"	0.90	.36	-	"	65	
-2.506	0.479	2.941	"	1.11	.36	-	"	45	
-2.546	"	2.893	"	-	.39	-	"	75	
-2.575	"	2.893	"	-	.36	-	"	55	
-2.548	0.509	2.862	"	0.94	.38	-	"	45	
-2.612	"	2.922	"	0.46	.27	-	"	65	
-2.643	"	2.744	"	-	.34	-	"	75	
-2.612	0.540	2.893	"	-	.36	-	"	"	

Cont'd. . . . . .

TABLE 5 (cont.)

316 Stainless Steel (3) log σ/E	T/T_m	log t_f (sec.)	$\dot{\epsilon}_{ss}$ (sec^{-1})	ln A_o/A_f	ln l_f/l_o	Fracture Type	Testing Mode	Grain Dia. (μm.)	Reference
-2.650	0.540	2.839	5.5×10^{-4}*	-	.32	-	CDR	55	Simmons and
-2.779	0.555	2.976	"	1.05	.42	-	"	65	Van Echo (1965)
-2.704	0.571	2.950	"	-	.40	-	"	75	Cont'd.
-2.779	0.601	2.992	"	1.18	.48	-	"	65	
-2.830	"	2.839	"	-	.32	-	"	55	
-2.972	"	3.045	"	-	.43	-	"	75	
-2.868	0.632	3.030	"	-	.46	-	"	"	
-3.146	0.663	3.086	"	0.94	.51	-	"	110	
-3.163	"	3.086	"	0.92	.51	-	"	"	
-3.072	0.693	2.872	"	-	.34	-	"	75	
-3.464	0.724	3.052	"	0.63	.46	-	"	110	
-3.473	"	3.023	"	0.62	.48	-	"	"	
-3.323	0.755	3.189	"	-	.62	-	"	75	
-3.673	0.786	3.135	"	0.67	.56	-	"	110	
-3.819	0.847	3.233	"	1.90	.66	-	"	"	
-3.819	"	3.214	"	1.66	.64	-	"	"	
-2.545	0.417	2.556	-	-	.35	-	CREEP+	88	
-2.550	"	>6.56	1.1×10^{-9}	-	-	-	"	"	

316 Stainless Steel (4) log σ/E	T/T_m	log t_f (sec.)	$\dot{\epsilon}_{ss}$ (sec^{-1})	ln A_o/A_f	ln l_f/l_o	Fracture Type	Testing Mode	Grain Dia. (μm.)	Reference
-2.554	0.463	4.565	-	-	.36	-	CREEP	88	Simmons and
-2.575	"	4.718	1.8×10^{-6}	-	.30	-	"	"	Van Echo (1965)
-2.654	"	5.614	7.2×10^{-8}	-	.26	-	"	"	Cont'd.
-2.700	"	5.993	2.8×10^{-8}	-	.13	-	"	"	
-2.755	"	6.613	5.2×10^{-9}	-	.10	-	"	"	
-2.685	0.479	4.247	4.0×10^{-6}	-	.27	-	"	43	
-2.725	"	4.680	1.6×10^{-6}	-	.22	-	"	"	
-2.765	"	5.128	5.2×10^{-7}	-	.20	-	"	"	
-2.805	"	5.577	1.6×10^{-7}	-	.17	-	"	"	
-2.845	"	6.201	5.4×10^{-8}	-	.21	-	"	"	
-2.885	"	6.799	1.1×10^{-8}	-	.17	-	"	"	
-2.567	"	4.238	2.1×10^{-6}	-	.35	-	"	62	
-2.582	"	4.486	9.1×10^{-7}	-	.22	-	"	"	
-2.597	"	4.621	8.0×10^{-7}	-	.22	-	"	"	
-2.613	"	4.724	6.0×10^{-7}	-	.23	-	"	"	
-2.664	"	5.136	-	-	.16	-	"	"	
-2.743	"	5.768	3.2×10^{-7}	-	.11	-	"	"	
-2.789	"	6.329	7.1×10^{-9}	-	.11	-	"	"	
-2.947	"	>7.033	2.8×10^{-10}	-	-	-	"	"	

Cont'd. . . . . .

TABLE 5 (cont.)

316 Stainless Steel (5) log σ/E	T/T_m	log t_f (sec.)	$\dot{\epsilon}_{ss}$ ($sec.^{-1}$)	ln A_o/A_f	ln l_f/l_o	Fracture Type	Testing Mode	Grain Dia. (μm.)	Reference
-2.743	0.479	5.994	-	-	.12	-	CREEP	43	Simmons and
-2.766	"	6.153	-	-	.12	-	"	"	Van Echo (1965)
-2.814	"	7.755	-	-	.04	-	"	"	Cont'd.
-2.676	0.509	3.971	1.7×10^{-5}	-	.30	-	"	88	
-2.750	"	4.622	3.5×10^{-6}	-	.32	-	"	"	
-2.785	"	5.227	1.1×10^{-6}	-	.36	-	"	"	
-2.852	"	5.782	1.7×10^{-7}	-	.34	-	"	"	
-2.940	"	6.339	4.2×10^{-8}	-	.22	-	"	"	
-2.838	"	5.247	-	-	.18	-	"	-	
-2.597	"	3.100	-	-	.24	-	"	52	
-2.686	"	3.937	-	-	.15	-	"	"	
-2.750	"	4.573	-	-	.13	-	"	"	
-2.931	"	6.549	-	-	.14	-	"	"	
-3.099	"	7.672	-	-	.09	-	"	"	
-2.898	"	5.382	-	-	.12	-	"	43	
-2.949	"	6.045	-	-	.11	-	"	"	
-2.987	"	6.793	-	-	.06	-	"	"	
-3.028	"	7.300	-	-	.04	-	"	"	

316 Stainless Steel (6) log σ/E	T/T_m	log t_f (sec.)	$\dot{\epsilon}_{ss}$ ($sec.^{-1}$)	ln A_o/A_f	ln l_f/l_o	Fracture Type	Testing Mode	Grain Dia. (μm.)	Reference
-2.882	0.509	5.459	-	-	.12	-	CREEP	-	Simmons and
-2.914	"	5.729	-	-	.11	-	"	-	Van Echo (1965)
-2.949	"	6.210	-	-	.11	-	"	-	Cont'd.
-2.987	"	6.695	-	-	.13	-	"	-	
-2.999	0.525	5.735	-	-	.23	-	"	-	
-2.913	0.540	4.542	8.2×10^{-6}	-	.60	-	"	43	
-2.983	"	5.038	2.4×10^{-6}	-	.68	-	"	"	
-3.052	"	5.610	8.0×10^{-7}	-	.68	-	"	"	
-3.123	"	6.087	2.8×10^{-7}	-	.73	-	"	"	
-3.192	"	6.511	9.4×10^{-8}	-	.64	-	"	"	
-3.262	"	6.842	3.3×10^{-8}	-	.52	-	"	"	
-3.333	"	7.133	1.2×10^{-8}	-	.35	-	"	"	
-2.669	"	2.918	-	-	.31	-	"	52	
-2.769	"	3.954	-	-	.29	-	"	"	
-2.808	"	4.401	-	-	.25	-	"	"	
-2.970	"	6.019	-	-	.26	-	"	"	
-3.034	"	6.383	-	-	.22	-	"	"	
-3.082	"	6.724	-	-	.17	-	"	"	

Cont'd. . . . . .

TABLE 5 (cont.)

316 Stainless Steel (7) log σ/E	T/T_m	log t_f (sec.)	$\dot{\epsilon}_{ss}$ (sec^{-1})	ln A_o/A_f	ln l_f/l_o	Fracture Type	Testing Mode	Grain Dia. (μm)	Reference
-2.711	0.540	3.356	1.1×10^{-4}	-	.43	-	CREEP	62	Simmons and
-2.745	"	4.136	1.3×10^{-5}	-	.44	-	"	"	Van Echo (1965)
-2.808	"	4.643	3.1×10^{-6}	-	.38	-	"	"	Cont'd.
-2.933	"	5.525	4.3×10^{-7}	-	.52	-	"	"	
-3.012	"	6.071	1.2×10^{-7}	-	.60	-	"	"	
-3.049	0.555	5.529	-	-	.48	-	"	"	
-2.804	0.571	3.475	-	-	.35	-	"	52	
-2.856	"	3.879	-	-	.36	-	"	"	
-2.934	"	4.389	-	-	.33	-	"	"	
-3.149	"	5.961	-	-	.30	-	"	"	
-3.254	"	6.550	-	-	.21	-	"	"	
-3.420	"	7.358	-	-	.10	-	"	"	
-3.146	0.601	4.483	9.9×10^{-6}	-	.71	-	"	44	
-3.247	"	5.059	2.9×10^{-6}	-	.67	-	"	"	
-3.347	"	5.604	6.9×10^{-7}	-	.55	-	"	"	
-3.427	"	6.003	2.5×10^{-7}	-	.45	-	"	"	
-3.545	"	6.470	5.8×10^{-8}	-	.33	-	"	"	
-3.647	"	6.811	-	-	.36	-	"	"	

316 Stainless Steel (8) log σ/E	T/T_m	log t_f (sec.)	$\dot{\epsilon}_{ss}$ (sec^{-1})	ln A_o/A_f	ln l_f/l_o	Fracture Type	Testing Mode	Grain Dia. (μm)	Reference
-3.746	0.601	7.218	-	-	.31	-	CREEP	44	Simmons and
-2.879	"	3.125	-	-	.44	-	"	58	Van Echo (1965)
-2.976	"	3.835	-	-	.40	-	"	"	Cont'd.
-3.073	"	4.454	-	-	.39	-	"	"	
-3.300	"	6.050	-	-	.29	-	"	"	
-3.408	"	6.469	-	-	.19	-	"	"	
-3.578	"	7.010	4.4×10^{-11}	-	.17	-	"	"	
-2.897	"	3.158	2.5×10^{-4}	-	.60	-	"	62	
-2.976	"	3.812	4.0×10^{-5}	-	.62	-	"	"	
-3.198	"	5.190	1.6×10^{-6}	-	.65	-	"	"	
-3.323	"	5.956	2.5×10^{-7}	-	.54	-	"	"	
-3.402	"	6.427	5.9×10^{-8}	-	.22	-	"	"	
-3.236	"	5.003	-	-	.29	-	"	-	
-3.323	"	5.304	-	-	.29	-	"	-	
-3.432	"	5.823	-	-	.25	-	"	-	
-3.537	"	6.609	-	-	.31	-	"	-	
-3.596	"	6.810	-	-	.29	-	"	-	
-3.407	0.632	5.556	-	-	-	-	"	52	
-3.632	"	6.556	-	-	-	-	"	"	

TABLE 5 (cont.)

316 Stainless Steel (9) log σ/E	T/T_m	log t_f (sec.)	$\dot{\epsilon}_{ss}$ ($sec.^{-1}$)	ln A_o/A_f	ln l_f/l_o	Fracture Type	Testing Mode	Grain Dia. (μm.)	Reference
-2.700	0.478	4.250	4.0×10^{-6}	-	.27	GBC/w †	CLC+	44	Garafalo et
-2.740	"	4.680	1.6×10^{-6}	-	.22	"	"	"	al. (1961a)
-2.780	"	5.130	5.2×10^{-7}	-	.20	"	"	"	
-2.820	"	5.580	1.6×10^{-7}	-	.17	"	"	"	
-2.860	"	6.200	5.4×10^{-8}	-	.21	"	"	"	
-2.900	"	6.800	1.1×10^{-8}	-	.17	"	"	"	
-2.860	0.540	3.890	3.5×10^{-5}	-	.53	GBC/w + r ††	"	"	
-2.930	"	4.540	8.2×10^{-6}	-	.60	"	"	"	
-3.000	"	5.090	2.3×10^{-6}	-	.67	"	"	"	
-3.070	"	5.610	8.0×10^{-7}	-	.68	"	"	"	
-3.140	"	6.090	2.8×10^{-7}	-	.73	"	"	"	
-3.210	"	6.510	9.4×10^{-8}	-	.63	"	"	"	
-3.280	"	6.840	3.3×10^{-8}	-	.52	"	"	"	
-3.350	"	7.130	1.2×10^{-8}	-	.35	"	"	"	
-3.060	0.601	3.840	4.3×10^{-5}	-	.70	"	"	"	
-3.160	"	4.480	9.9×10^{-6}	-	.70	"	"	"	
-3.260	"	5.060	2.9×10^{-6}	-	.67	"	"	"	
-3.360	"	5.600	6.9×10^{-7}	-	.55	"	"	"	
-3.440	"	6.000	2.4×10^{-7}	-	.45	"	"	"	

316 Stainless Steel (10) log σ/E	T/T_m	log t_f (sec.)	$\dot{\epsilon}_{ss}$ ($sec.^{-1}$)	ln A_o/A_f	ln l_f/l_o	Fracture Type	Testing Mode	Grain Dia. (μm.)	Reference
-3.560	0.601	6.470	5.9×10^{-8}	-	.33	GBC/w + r	CLC	44	Garofalo et
-3.660	"	6.810	-	-	.36	"	"	"	al. (1961 a)
-3.760	"	7.220	-	-	.31	"	"	"	Cont'd.
-2.660	0.479	4.150	1.1×10^{-5}	.74	.43	-	"	50§	Garofalo et
-2.700	"	5.080	-	.23	.22	-	"	"	al. (1961b)
-2.750	"	5.730	7.2×10^{-8}	.28	.18	-	"	"	
-2.800	"	5.900	-	.15	.10	-	"	"	
-2.850	"	6.530	-	.23	.15	-	"	"	
-2.910	"	7.170	-	.29	.14	-	"	"	
-2.810	0.540	3.880	4.1×10^{-5}	.93	.51	-	"	"	
-2.920	"	4.860	2.8×10^{-6}	1.00	.57	-	"	"	
-3.020	"	5.630	3.9×10^{-7}	.97	.63	-	"	"	
-3.040	"	5.680	5.3×10^{-7}	1.33	.68	-	"	"	
-3.140	"	6.290	1.1×10^{-7}	.70	.53	-	"	"	
-3.210	"	6.590	3.3×10^{-8}	.57	.46	-	"	"	
-3.030	0.601	3.810	6.4×10^{-5}	1.06	.67	-	"	"	
-3.170	"	4.670	7.3×10^{-6}	1.04	.71	-	"	"	
-3.290	"	5.430	-	1.17	.79	-	"	"	

Cont'd. . . . . .

TABLE 5 (cont.)

316 Stainless Steel (11) log σ/E	T/T_m	log t_f (sec.)	$\dot{\epsilon}_{ss}$ (sec^{-1})	ln A_o/A_f	ln l_f/l_o	Fracture Type	Testing Mode	Grain Dia. (μm)	Reference
-3.410	0.601	6.130	-	.88	.70	-	CLC	50	Garofalo et
-3.550	"	6.740	-	.41	.37	-	"	"	al (1961b) Cont'd.
-2.570	0.164	-	-	1.51	.50	-	CDR	44	Smith et al (1950)
-2.560	0.479	-	-	.87	.36	-	"	"	
-2.670	0.540	-	-	.69	.32	-	"	"	
-2.850	0.602	-	-	.56	.32	-	"	"	
-2.610	0.479	3.60	5.6×10^{-6}	.98	.36	TG++	CLC	"	
-2.630	"	4.22	1.8×10^{-6}	.54	.33	"	"	"	
-2.660	"	4.49	7.9×10^{-7}	.33	.23	IG++	"	"	
-2.670	"	4.640	6.9×10^{-7}	.30	.21	"	"	"	
-2.700	"	4.760	5.2×10^{-7}	.33	.22	"	"	"	
-2.730	"	5.140	3.7×10^{-7}	.22	.15	"	"	"	
-2.810	"	5.770	3.0×10^{-8}	.25	.12	"	"	"	
-2.860	"	6.360	6.5×10^{-9}	.17	.12	"	"	"	
-2.760	0.540	3.360	-	.87	.43	TG++	"	"	
-2.770	"	4.070	1.3×10^{-5}	.89	.43	"	"	"	
-2.840	"	4.660	3.2×10^{-6}	.71	.37	IG++	"	"	
-2.950	"	5.470	4.0×10^{-7}	.98	.49	"	"	"	

316 Stainless Steel (12) log σ/E	T/T_m	log t_f (sec.)	$\dot{\epsilon}_{ss}$ (sec^{-1})	ln A_o/A_f	ln l_f/l_o	Fracture Type	Testing Mode	Grain Dia. (μm)	Reference
-3.070	0.540	6.160	1.4×10^{-7}	.91	.58	IG++	CLC	44	Smith et al (1950)
-2.900	0.602	2.960	-	1.37	.58	TG++	"	"	Cont'd.
-2.900	"	3.190	-	1.29	.60	"	"	"	
-2.950	"	3.790	-	1.12	.59	"	"	"	
-3.190	"	5.160	1.7×10^{-6}	1.18	.64	IG++	"	"	
-3.330	"	6.000	2.6×10^{-7}	.72	.51	"	"	"	
-3.430	"	6.420	5.4×10^{-8}	.38	.24	"	"	"	
-2.183	0.013	-	-	-	.44	-	CDR	-	INCO (1974)
-2.261	0.040	-	-	.96	.46	-	"	-	
-2.328	0.068	-	-	1.11	.48	-	"	-	
-2.396	0.096	-	-	1.27	.49	-	"	-	
-2.475	0.123	-	-	1.39	.51	-	"	-	
-2.520	0.151	-	-	1.42	.51	-	"	-	
-2.556	0.165	-	-	1.47	.51	-	"	-	
-2.810	0.455	7.560	-	-	-	-	CREEP	-	ISO (1969)
-2.830	"	8.030	-	-	-	-	"	-	
-2.870	"	8.260	-	-	-	-	"	-	
-2.830	0.460	7.560	-	-	-	-	"	-	

Cont'd. . . . . .

TABLE 5 (cont.)

316 Stainless Steel (13) log σ/E	T/T_m	log t_f (sec.)	$\dot{\epsilon}_{ss}$ ($sec.^{-1}$)	ln A_o/A_f	ln l_f/l_o	Fracture Type	Testing Mode	Grain Dia. (μm.)	Reference
-2.870	0.460	8.030	-	-	-	-	CREEP	-	ISO (1969)
-2.900	"	8.260	-	-	-	-	"	-	Cont'd.
-2.860	0.466	7.560	-	-	-	-	"	-	
-2.910	"	8.030	-	-	-	-	"	-	
-2.930	"	8.260	-	-	-	-	"	-	
-2.890	0.471	7.560	-	-	-	-	"	-	
-2.940	"	8.030	-	-	-	-	"	-	
-2.970	"	8.260	-	-	-	-	"	-	
-3.050	"	8.560	-	-	-	-	"	-	
-3.070	"	8.730	-	-	-	-	"	-	
-3.090	"	8.860	-	-	-	-	"	-	
-2.920	0.477	7.560	-	-	-	-	"	-	
-2.980	"	8.030	-	-	-	-	"	-	
-3.010	"	8.260	-	-	-	-	"	-	
-3.090	"	8.560	-	-	-	-	"	-	
-3.120	"	8.730	-	-	-	-	"	-	
-3.150	"	8.860	-	-	-	-	"	-	
-2.950	0.482	7.560	-	-	-	-	"	-	

316 Stainless Steel (14) log σ/E	T/T_m	log t_f (sec.)	$\dot{\epsilon}_{ss}$ ($sec.^{-1}$)	ln A_o/A_f	ln l_f/l_o	Fracture Type	Testing Mode	Grain Dia. (μm.)	Reference
-3.020	0.482	8.030	-	-	-	-	CREEP	-	ISO (1969)
-3.050	"	8.260	-	-	-	-	"	-	Cont'd.
-3.130	"	8.560	-	-	-	-	"	-	
-3.170	"	8.730	-	-	-	-	"	-	
-3.190	"	8.860	-	-	-	-	"	-	
-2.990	0.488	7.560	-	-	-	-	"	-	
-3.060	"	8.030	-	-	-	-	"	-	
-3.100	"	8.260	-	-	-	-	"	-	
-3.180	"	8.560	-	-	-	-	"	-	
-3.220	"	8.730	-	-	-	-	"	-	
-3.240	"	8.860	-	-	-	-	"	-	
-3.030	0.493	7.560	-	-	-	-	"	-	
-3.100	"	8.030	-	-	-	-	"	-	
-3.140	"	8.260	-	-	-	-	"	-	
-3.220	"	8.560	-	-	-	-	"	-	
-3.270	"	8.730	-	-	-	-	"	-	
-3.300	"	8.860	-	-	-	-	"	-	
-3.060	0.499	7.560	-	-	-	-	"	-	Cont'd. . . . .

TABLE 5 (cont.)

316 Stainless Steel (15) log σ/E	T/T_m	log t_f (sec.)	$\dot{\epsilon}_{ss}$ (sec.$^{-1}$)	ln A_o/A_f	ln l_f/l_o	Fracture Type	Testing Mode	Grain Dia. (μm.)	Reference
-3.150	0.499	8.030	-	-	-	-	CREEP	-	ISO (1969)
-3.190	"	8.260	-	-	-	-	"	-	Cont'd.
-3.260	"	8.560	-	-	-	-	"	-	
-3.320	"	8.730	-	-	-	-	"	-	
-3.350	"	8.860	-	-	-	-	"	-	
-3.110	0.504	7.560	-	-	-	-	"	-	
-3.200	"	8.030	-	-	-	-	"	-	
-3.240	"	8.260	-	-	-	-	"	-	
-3.310	"	8.560	-	-	-	-	"	-	
-3.360	"	8.730	-	-	-	-	"	-	
-3.400	"	8.860	-	-	-	-	"	-	
-3.150	0.510	7.560	-	-	-	-	"	-	
-3.240	"	8.030	-	-	-	-	"	-	
-3.290	"	8.260	-	-	-	-	"	-	
-3.350	"	8.560	-	-	-	-	"	-	
-3.410	"	8.730	-	-	-	-	"	-	
-3.440	"	8.830	-	-	-	-	"	-	
-3.190	0.516	7.560	-	-	-	-	"	-	

316 Stainless Steel (16) log σ/E	T/T_m	log t_f (sec.)	$\dot{\epsilon}_{ss}$ (sec.$^{-1}$)	ln A_o/A_f	ln l_f/l_o	Fracture Type	Testing Mode	Grain Dia. (μm.)	Reference
-3.290	0.516	8.030	-	-	-	-	CREEP	-	ISO (1969)
-3.330	"	8.260	-	-	-	-	"	-	Cont'd.
-3.410	"	8.560	-	-	-	-	"	-	
-3.470	"	8.730	-	-	-	-	"	-	
-3.500	"	8.830	-	-	-	-	"	-	
-3.240	0.521	7.560	-	-	-	-	"	-	
-3.330	"	8.030	-	-	-	-	"	-	
-3.390	"	8.260	-	-	-	-	"	-	
-3.460	"	8.560	-	-	-	-	"	-	
-3.510	"	8.730	-	-	-	-	"	-	
-3.550	"	8.860	-	-	-	-	"	-	
-3.280	0.527	7.560	-	-	-	-	"	-	
-3.380	"	8.030	-	-	-	-	"	-	
-3.440	"	8.260	-	-	-	-	"	-	
-3.520	"	8.560	-	-	-	-	"	-	
-3.570	"	8.730	-	-	-	-	"	-	
-3.600	"	8.860	-	-	-	-	"	-	
-3.310	0.532	7.560	-	-	-	-	"	-	
									Cont'd. . . . .

TABLE 5 (cont.)

316 Stainless Steel (17) log σ/E	T/T_m	log t_f (sec.)	$\dot{\epsilon}_{ss}$ ($sec.^{-1}$)	ln A_o/A_f	ln l_f/l_o	Fracture Type	Testing Mode	Grain Dia. (μm.)	Reference
-3.430	0.532	8.030	-	-	-	-	CREEP	-	ISO (1969)
-3.480	"	8.260	-	-	-	-	"	-	Cont'd.
-3.570	"	8.560	-	-	-	-	"	-	
-3.370	0.538	7.560	-	-	-	-	"	-	
-3.470	"	8.030	-	-	-	-	"	-	
-3.520	"	8.260	-	-	-	-	"	-	
-3.610	"	8.560	-	-	-	-	"	-	
-3.400	0.543	7.560	-	-	-	-	"	-	
-3.510	"	8.030	-	-	-	-	"	-	
-3.580	"	8.260	-	-	-	-	"	-	
-3.660	"	8.560	-	-	-	-	"	-	
-3.450	0.549	7.560	-	-	-	-	"	-	
-3.560	"	8.030	-	-	-	-	"	-	
-3.620	"	8.260	-	-	-	-	"	-	
-3.690	"	8.560	-	-	-	-	"	-	
-3.490	0.554	7.560	-	-	-	-	"	-	
-3.520	0.560	7.560	-	-	-	-	"	-	
-3.570	0.565	7.560	-	-	-	-	"	-	

316 Stainless Steel (18) log σ/E	T/T_m	log t_f (sec.)	$\dot{\epsilon}_{ss}$ ($sec.^{-1}$)	ln A_o/A_f	ln l_f/l_o	Fracture Type	Testing Mode	Grain Dia. (μm.)	Reference
-2.483	0.510	-	1.7×10^{-1}	0.96	-	TG	CDR	100	Wray (1969)
-2.457	"	-	2.8×10^{-2}	1.33	-	"	"	"	
-2.470	"	-	"	1.34	-	"	"	"	
-2.470	"	-	1.1×10^{-2}	1.26	-	"	"	"	
-2.480	"	-	2.8×10^{-3}	1.29	0.36	"	"	"	
-2.472	"	-	8.3×10^{-4}	-	-	"	"	"	
-2.491	"	-	2.8×10^{-4}	1.09	-	GBC §§	"	"	
-2.528	"	-	8.3×10^{-5}	0.93	-	"	"	"	
-2.585	"	-	2.1×10^{-5}	0.63	-	"	"	"	
-2.523	0.538	-	1.7×10^{-1}	1.21	-	TG	"	"	
-2.496	"	-	"	1.46	-	"	"	"	
-2.491	"	-	"	1.43	-	"	"	"	
-2.536	"	-	8.3×10^{-2}	1.46	-	"	"	"	
-2.506	"	-	"	1.53	-	"	"	"	
-2.493	"	-	2.8×10^{-2}	1.47	-	"	"	"	
-2.500	"	-	1.7×10^{-2}	1.30	-	-	"	"	
-2.507	"	-	1.1×10^{-2}	1.23	-	-	"	"	
-2.513	"	-	"	1.46	-	-	"	"	
									Cont'd. . . . .

TABLE 5 (cont.)

316 Stainless Steel (19) log σ/E	T/T_m	log t_f (sec.)	$\dot{\epsilon}_{ss}$ (sec^{-1})	ln A_o/A_f	ln l_f/l_o	Fracture Type	Testing Mode	Grain Dia. (μm.)	Reference
-2.511	0.538	-	8.3×10^{-3}	1.31	-	TG	CDR	100	Wray (1969)
-2.525	"	-	4.2×10^{-3}	1.36	-	GBC §§	"	"	Cont'd.
-2.542	"	-	1.7×10^{-3}	1.24	0.42	"	"	"	
-2.584	"	-	5.9×10^{-4}	-	-	-	"	"	
-2.584	"	-	3.1×10^{-4}	1.16	-	GBC §§	"	"	
-2.602	"	-	"	0.89	-	-	"	"	
-2.607	"	-	1.7×10^{-4}	1.20	-	-	"	"	
-2.638	"	-	8.3×10^{-5}	1.14	-	-	"	"	
-2.702	"	-	2.1×10^{-5}	1.14	-	GBC §§	"	"	
-2.539	0.571	-	1.7×10^{-1}	1.42	-	TG	"	"	
-2.573	"	-	2.8×10^{-2}	1.36	-	"	"	"	
-2.581	"	-	1.1×10^{-2}	-	-	"	"	"	
-2.610	"	-	2.8×10^{-3}	-	0.57	GBC §§	"	"	
-2.622	"	-	"	-	-	"	"	"	
-2.721	"	-	2.8×10^{-4}	-	-	"	"	"	
-2.847	"	-	2.8×10^{-5}	-	-	-	"	"	
-2.711	0.601	-	2.8×10^{-3}	-	0.57	TG	"	"	
-	0.632	-	1.7×10^{-1}	1.24	-	TG	"	"	

316 Stainless Steel (20) log σ/E	T/T_m	log t_f (sec.)	$\dot{\epsilon}_{ss}$ (sec^{-1})	ln A_o/A_f	ln l_f/l_o	Fracture Type	Testing Mode	Grain Dia. (μm.)	Reference
-2.686	0.632	-	2.8×10^{-2}	1.17	-	TG	CDR	100	Wray (1969)
-2.802	"	-	2.8×10^{-3}	0.80	0.57	"	"	"	Cont'd.
-3.123	"	-	2.1×10^{-5}	-	-	"	"	"	
-2.516	0.540	-	1.1×10^{-3}	1.36	0.36	-	CSC +	"	
-2.533	"	-	9.2×10^{-4}	1.13	0.40	-	"	"	
-2.551	"	-	4.0×10^{-4}	1.15	0.32	-	"	"	
-2.583	"	-	2.5×10^{-4}	1.00	0.46	-	"	"	
-2.585	"	-	3.9×10^{-4}	1.19	0.43	-	"	"	
-2.625	"	-	1.6×10^{-4}	0.27	0.24	IG **	"	"	
-2.625	"	-	1.5×10^{-4}	0.25	0.24	IG **	"	"	
-2.625	"	-	-	0.40	0.24	-	"	"	
-2.630	"	-	1.6×10^{-4}	0.79	0.44	-	"	"	
-2.695	"	-	1.8×10^{-5}	1.19	0.45	-	"	"	
-2.760	"	-	5.3×10^{-6}	0.39	0.30	-	"	"	
-2.815	"	-	4.7×10^{-4}	0.22	0.34	IG **	"	"	
-2.815	"	-	4.7×10^{-4}	-	0.39	-	"	"	
-2.630	"	-	-	0.16	0.25	IG**	"	"	
-2.630	"	-	-	0.21	0.33	IG **	"	"	
									Cont'd. . . . .

TABLE 5 (cont.)

316 Stainless Steel (21) log σ/E	T/T_m	log t_f (sec.)	$\dot{\epsilon}_{ss}$ (sec^{-1})	ln A_o/A_f	ln l_f/l_o	Fracture Type	Testing Mode	Grain Dia. (μm.)	Reference
-2.630	0.540	-	-	0.26	0.38	IG**	CSC	100	Wray (1969)
-2.630	"	-	6.7×10^{-5}	-	0.39	-	"	"	Cont'd.
-2.727	"	-	1.0×10^{-5}	-	0.35	-	"	"	
-2.727	"	-	1.2×10^{-5}	-	0.42	-	"	"	

+ CDR - constant displacement-rate tensile test; CLC - constant load, uniaxial creep test; CSC - constant stress, uniaxial creep test; CREEP - unspecified loading mode, uniaxial creep test.
* This strain-rate was assumed for these tensile tests in order to calculate a time-to-failure from the longitudinal fracture strain.
† Grain boundary cavitation of w-type.
†† Grain boundary cavitation of w- and r-type.
++ TG (or IG) transgranular(or intergranular) fracture inferred from position in stress and time relative to kink in creep rupture curve.
** Deduced from ratio of area strain to longitudinal strain.
§ Grain size estimated from micrograph.
§§ Grain boundary cavitation observed, but was not necessarily the cause of final fracture.

3.2 Fracture-Mechanism Maps for 304 and 316

Little can be learned from the engineering studies about the mechanisms of fracture of these steels. The scientific study of 316 by Wray (1969) identified regimes of ductile fracture, of intergranular creep fracture and of rupture. We have combined fractographic information from Wray's (1969) work with observations and stress-rupture data from Smith et al (1950), Dulis et al (1953), Garofalo et al (1961 a. b.) and Sanderson et al (1969), together with our own observations and data, to give the two sorts of map shown in Figs. 4 to 8.

The advantage of the maps with stress and temperature as axes (Fig. 4 and 5) is that they cover the entire range of conditions for which the material is solid. The data of Tables 4 and 5 is plotted on them, as open symbols if the fracture was transgranular and as full symbols if it was intergranular.

We have identified the field boundary separating ductile transgranular fracture from transgranular creep fracture with the U.T.S. of the steel in normal tensile tests ($t_f < 10^2$ s). If the initial stress is greater than this, the material can be regarded as a (rate-independent) plastic solid which fails more or less instantaneously, in a ductile manner. If the initial stress is less than this, failure is not instantaneous, but requires the accumulation of creep strain. Though crude, this criterion is straight-forward and uses existing data: that of Sanderson et al (1969) Simmons et al (1965) and our own observations.

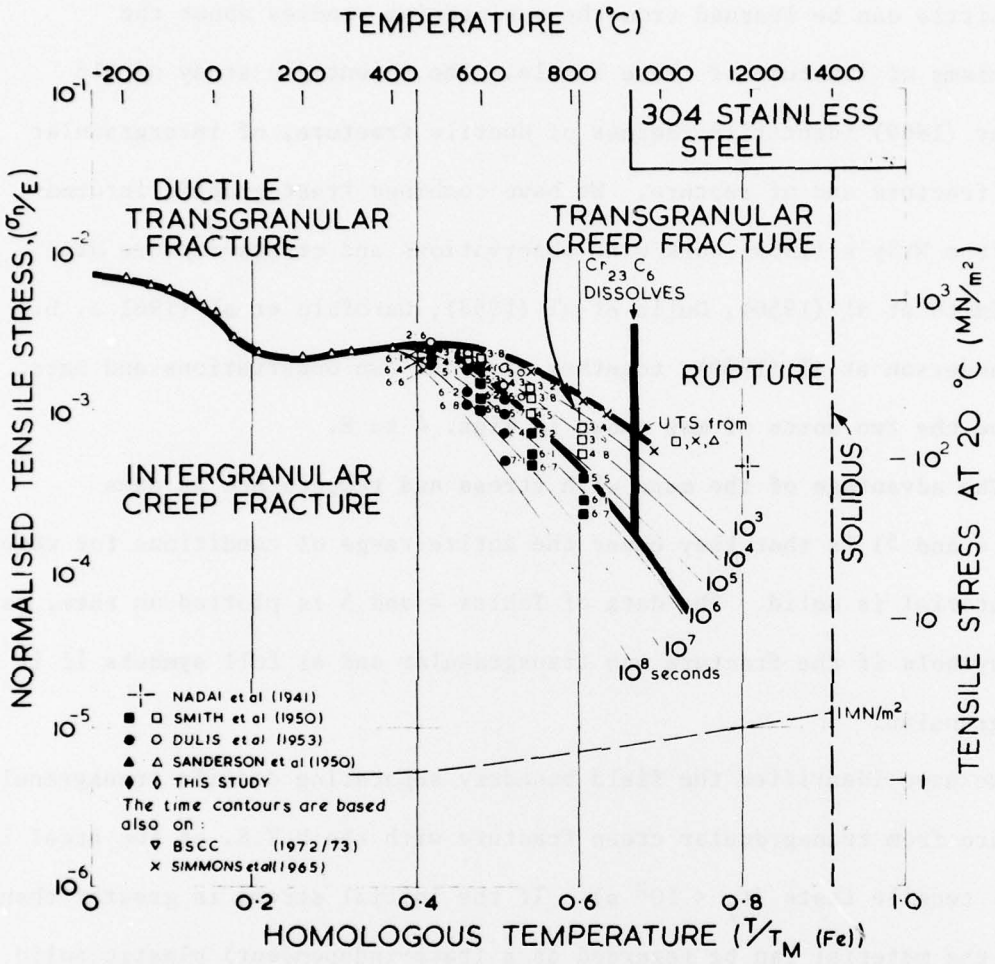

Fig. 4 A fracture map for type 304 stainless steel. It shows four mechanism fields. Contours of constant time-to-fracture (t_f) are shown. They are based on data from the sources listed on the figure.

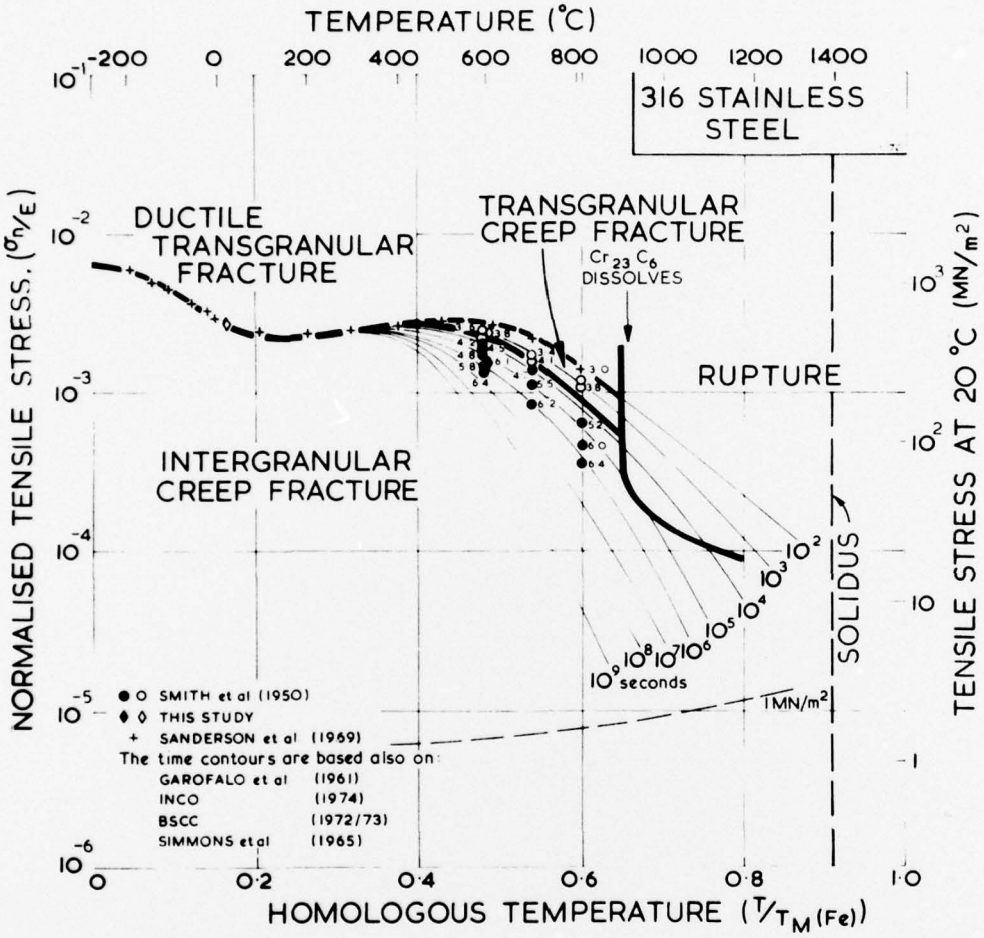

Fig. 5 A fracture map for type 316 stainless steel.

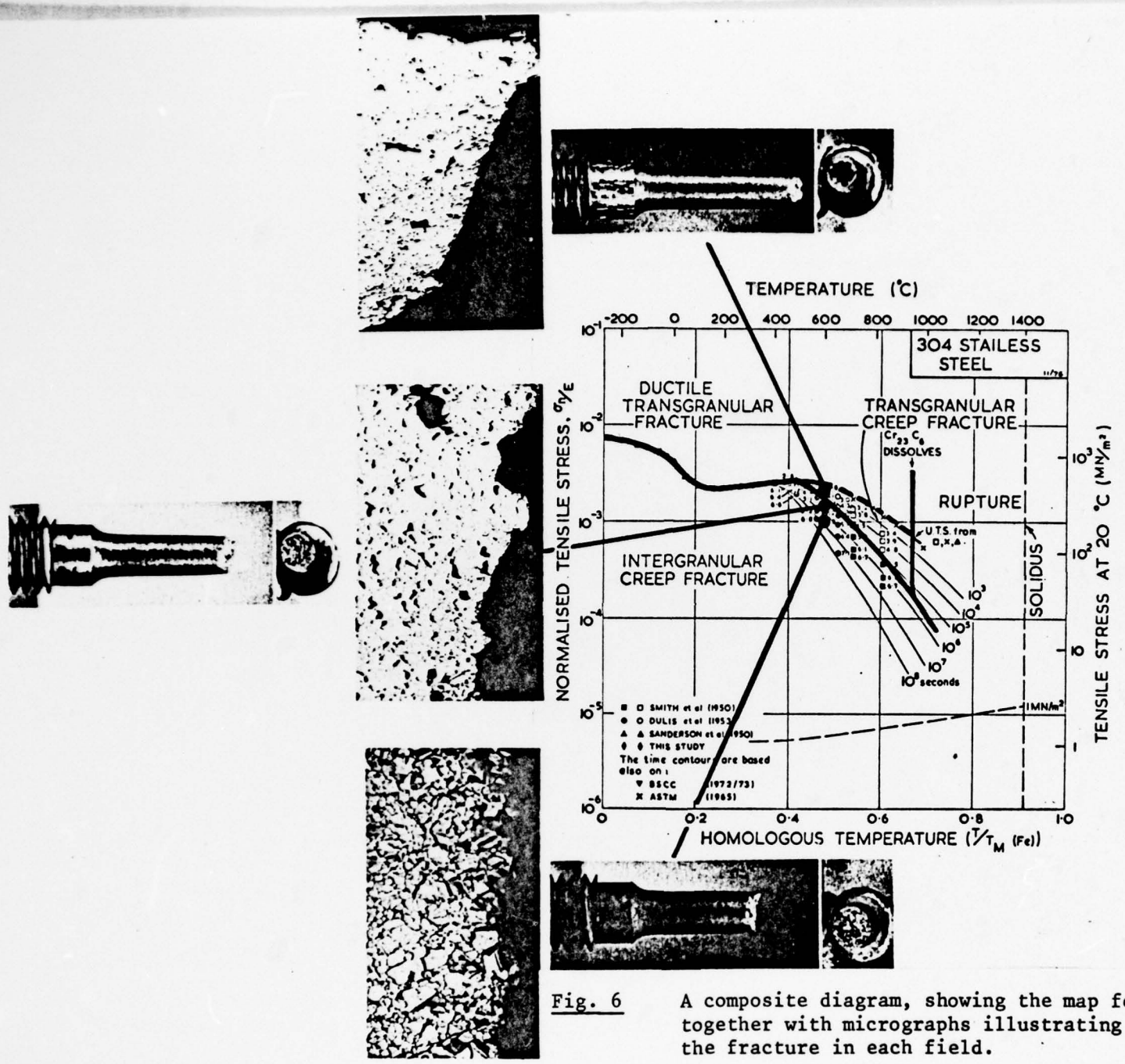

Fig. 6 A composite diagram, showing the map for 304 stainless steel, together with micrographs illustrating the characteristics of the fracture in each field.

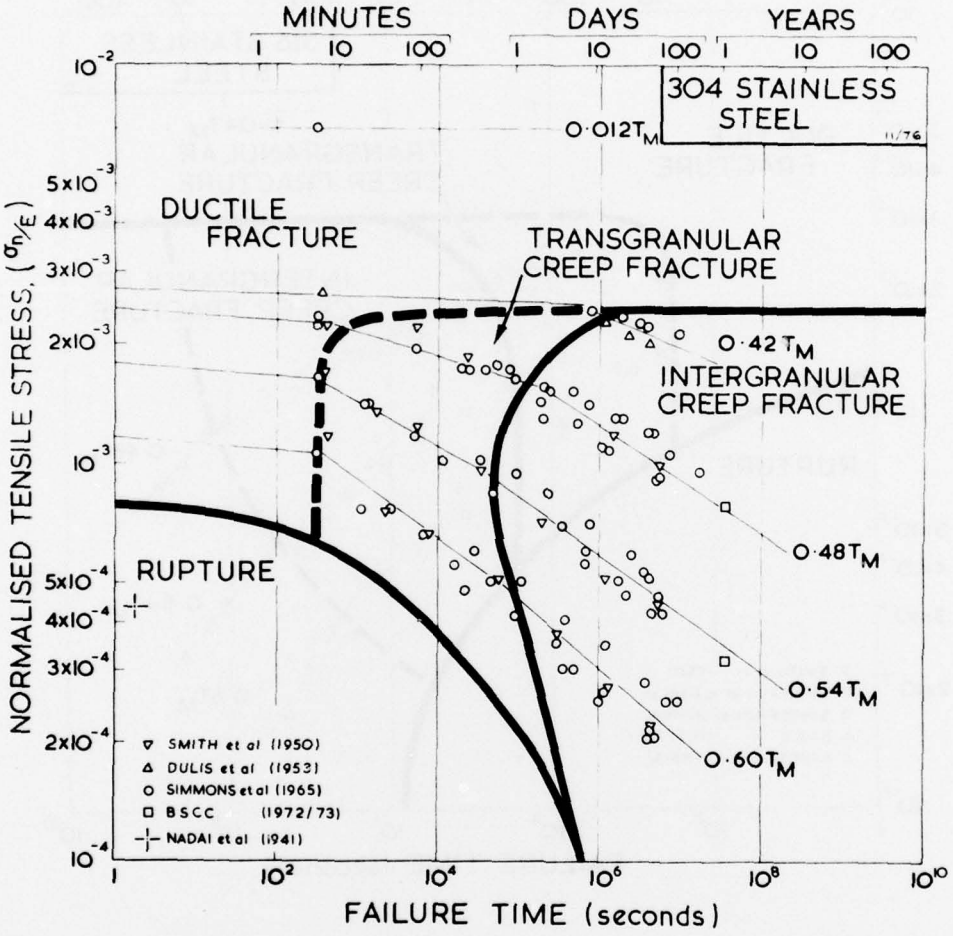

Fig. 7 A stress-rupture plot for 304 stainless steel. The field boundaries have been cross-plotted onto this figure from Fig. 4. Changes of slope of the stress-rupture plot coincide with changes in mechanism of fracture.

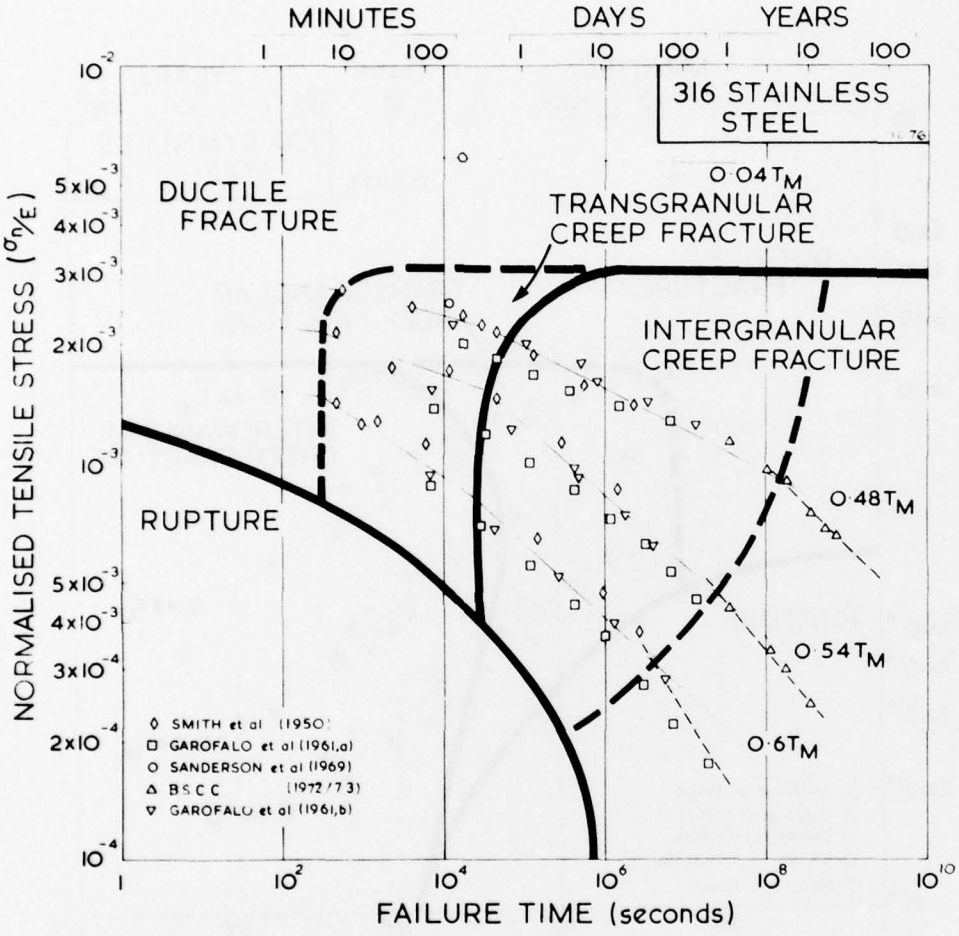

Fig. 8 A stress-rupture plot for 316 stainless steel. The field boundaries have been cross-plotted onto this figure from Fig. 5. There is an unexplained change of slope, and perhaps of mechanism, at long times.

The boundary separating intergranular from transgranular creep fracture on the two figures was positioned to be consistent with the observations of Smith et al (1950). Some of their micrographs for 304 are shown in Fig. 6, which illustrates the method. The uppermost group of pictures shows transgranular creep fracture. The sample has necked extensively, and internal cavities are elongated in the direction of tension. The central and lower groups of micrographs show intergranular fracture, little or no necking, and wedge cracks lying normal to the direction of tension. The figure illustrates that - on the axes used for these maps - this boundary is a fairly sharp one. Positioned in this way, the boundary coincides more or less exactly with a pronounced kink in the stress-rupture plots presented by Smith et al (1950).

Above about 900^{o}C (0.65 T_M), intergranular fracture in both 304 and 316 is suppressed; the steel necks extensively and fails by plastic rupture (Nadai and Manjoine 1941: Wray, 1969). This behaviour is common among commercially pure f.c.c. metals and alloys (Gandhi et al, 1977), where it appears to be associated with dynamic recrystallisation. In the stainless steels this, in turn, may be triggered by the solution of certain of the carbide precipitates: $M_{23}C_6$ carbides in 18-8 stainless steels are known to dissolve somewhere between 800 and 900 ^{o}C (Aborn and Bain, 1930).

An alternative way of presenting the data is shown in Figs. 7 and 8. Here the axes are those of the conventional stress-rupture plot: log (tensile stress) and log (time). Data obtained at one temperature is connected by a line and labelled with the temperature. The field-boundaries from the fracture maps of Figs. 4 and 5 have been cross-plotted onto Figs. 7 and 8, dividing stress-time space into fields in which (as before) a given mechanism of fracture is dominant.

The plots emphasise the way in which a change of mechanism is associated with a kink in the stress-rupture plot. That for 316 shows evidence for a new change of mechanism: about 10^7 seconds, the plots show unexplained kinks, through which we have drawn a heavy broken line. We have not yet been able

to examine specimens which have failed at these long times, and do not know whether it is the shape and distribution of the intergranular cracks which has changed (as they did in pure iron), or whether a change in precipitate distribution, caused by long aging under stress, has caused a change in the kinetics of intergranular cracking.

4. CONCLUSIONS

4.1 *Fracture maps for steels*

Observations of the fracture in tension of round bars of iron, or of a steel, can be summarised as a *fracture mechanism map*. The map shows the region of stress, time and temperatures over which a given mechanism of fracture is dominant. We have found that, although data was drawn from many different sources, there is little ambiguity in defining the boundaries of these regions or fields, and the resulting map gives a broad and self-consistent picture of the way the material behaves.

4.2 *Applications : extrapolation of creep-fracture data*

The law governing the creep life changes when the mechanism of fracture changes. An extrapolation procedure which is satisfactory within one field cannot be expected to properly describe the behaviour in an adjacent field. The field boundaries define the *limits of safe extrapolation.*

4.3 *Applications : guidance in scientific studies and in engineering design*

Each mechanism of fracture has its own characteristics: each depends in its own way on stress state, for example; and (in creep) the stress- and temperature-dependence of the time to fracture differs for each. In studying a particular mechanism, or in designing an engineering structure in such a way as to avoid it, it is helpful to know its region of dominance, and its characteristics. This study has attempted to provide this information for pure iron and for 304 and 316 stainless steel.

ACKNOWLEDGEMENTS

This work was supported by the U.S. Army under Contract Number DAERO-7-G-060. We are most grateful to Dr. P. J. Wray, of the U.S. Steels Research Centre, for his advice and help in providing unpublished data.

REFERENCES

Aborn, R.H. and Bain, E.C. (1930) Trans. Amer. Soc. Steel Treating 18, 837.

A.S.M. (1961) Metals Handbook, Volume 1.

Blackburn, L.D., *The Generation of Isochronous Stress Strain Curves*, A.S.M.E. Winter Annual Meeting, New York, Nov. 1972, Publisher A.S.M.E.

B.S.C.C. (1972/1973) British Steel Corporation ISO/TC17/SC10/ETP-SG (Secretariat 104) 138-MT/QF/54/74 page 11.

Cane, B.J. and Greenwood, G.W. (1975) Mat. Sci. Jnl. 9, 55.

Dever, D.J. (1972) J. Appl. Phys. 43, 3293.

Dulis, E.J., Smith, G.V. and Houston, E.G. (1953) Trans. A.S.M. 45, 42.

Fields, R.J. and Ashby, M.F. (1976) Phil. Mag. 33, 33.

Frost, H.J. and Ashby, M.F. (1975) *Deformation-Mechanism Maps for Pure Iron, Two Austenitic Stainless Steels and a Low-Alloy Ferritic Steel*, Cambridge University, Engineering Dept. Report, July

Garofalo, F. (1960) Proc. A.S.T.M. 60, 738.

Garofalo, F., Whitmore, R.W., Domis, W.F. and von Gemmingen, F. (1961a) Trans. Metall. Soc. A.I.M.E. 221, 310.

Garofalo, F., von Gemmingen, F. Domis, W.F. (1961b) Trans. A.S.M. 54, 430.

Gröschel, F. (1975) Diploma Thesis University of Erlangen ERAMS-1/TR.32.

I.N.C.O. (1974) Datasheet *Materials for Cryogenic Service: Austenitic Stainless Steels : Engineering Properties*, International Nickel Ltd., London.

Köster, W. (1948) Z. Metallkunde 9, 1.

Lai, J. (1977) Private communication.

Lord, A.E. and Beshers, D.N. (1964) J. Appl. Phys., 35, 2397.

Marshall, P. (1977) Private communication.

McMahon, C. and Cohen, M. (1965) Acta Met., 13, 591.

Nadai, A. and Manjoine, M.J. (1941), J. Appl. Mechanics 63, A-77.

Parr, J.G. and Hanson, A. (1965) *An Introduction to Stainless Steel* A.S.M., Metals Park, Ohio.

Sanderson, G.P. and Llewellyn, D.J. (1969) J.I.S.I., 207, 1129.

Smithells, C.J. (1967) Metals Reference Book, Butterworths vol. 3.

Simmons, W.F. and Cross, H.C. (1952) A.S.T.M. Spec. Tech. Pub. No. 124.

Simmons, W.J. and van Echo, J.A. (1965) A.S.T.M. Data Series Pub. DS5-S1.

Simonsen, E.B. and Dossin, J.M. (1965) J. Iron and Steel Inst., 203, 380.

Sleeswyk, A.W. (1961) Acta Met. 9, 32.

Smith, G.V., Dulis, E.J. and Houston, E.G. (1950) Trans. A.S.M. 42, 935.

Taplin, D.M.R. and Wingrove, A.L. (1967) Acta Met., 15, 1231.

Weiss, B. and Stickler, R. (1972) Met. Trans. 3, 851.

Westwood, H.J. (1976) private communication.

Westwood, H.J. and Taplin, D.M.R. (1974) private communication.

Wray, P.J. (1969) J. Appl. Phys. 40, 4018.

Wray, P.J. (1975) Met. Trans., 6A, 1379; (1975 a) Met. Trans. 6A, 1197.

Wray, P.J. (1977) private communication.

Wray, P.J. and Holmes, M.F. (1975) Metall. Trans., 6A, 1189.